

EXPERIMENTAL STUDY OF ALUMINUM SHEET SURFACE  
ROUGHNESS USING OPTICAL INTERFEROMETRY

by

Glenn Arthur Lucachick

B.S., University of North Dakota, 2008

A thesis submitted to the  
University of Colorado Denver  
in partial fulfillment  
of the requirements for the degree of  
Master of Science  
Mechanical Engineering

2011

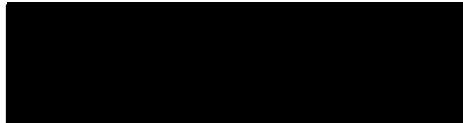
This thesis for the Master of Science

degree by

Glenn Arthur Lucachick

has been approved

by



---

Rafael Sanchez (ADVISOR)



---

John Trapp



---

Atousa Plaseied

April 20, 2011

---

Date



Lucachick, Glenn Arthur (M.S., Mechanical Engineering)

An optical interferometry investigation of the evolution of surface roughness during manufacturing process simulations

Thesis directed by Associate Professor Rafael Sanchez

### ABSTRACT

During sheet metal forming, the surface finish changes as the sheet slides, bends, and stretches against the tools. Specially engineered surface finishes have been developed by automakers to improve forming consistency and painting quality. This study assessed the evolution of surface parameters on aluminum sheet surface finishes during manufacturing processes.

The scope of this work is experimental. Two surface finish conditions were studied, mill finish (MF) and electro discharge texture (EDT). The 3D Surface roughness conditions were determined for these materials in both the longitudinal and the transverse rolling directions of the sheet. The sheets were tested using several tests (i) three pin Draw Bead Simulator (DBS) tests, with tests run under fix and roller conditions, (ii) pure bending moment tests, (iii) and tensile tests. A 3-D Wyko profilometer was used to take the surface roughness measurements.

The changes in surface roughness due to bending effects, tension effects, and contact effects are investigated for both material types and rolling

directions. The results indicate that the creation of new surface features during tensile straining under both bending and tension are more significant in influencing surface textures in MF sheet than in EDT sheet. During the initial change in curvature for DBS and pure bending moment tests from flat to concave the MF samples experienced an average increase in roughness 390% greater than EDT. This trend is observed in similar strain directions undertaken during the cycles investigated. Conversely, the effects of contact pressure and friction were found more influential for EDT surface textures than in MF at the middle pin. At that location, the transition from an uncontacted convex surface to a concave surface under DBS contact pressure results in a surface roughness 10% less than the starting value for EDT samples, whereas MF returns to approximately the original value.

This study showed changing trends on the surface roughness of sheet metal under bending and tension. It also shows a methodology to assess those roughness changes. The understanding of the contact effects on surface roughness for sheet textures may provide insight for further texture optimization and to the understanding of friction itself.

This abstract accurately represents the content of the candidate's thesis. I  
recommend its publication.

Signed, \_\_\_\_\_



Rafael Sanchez

## ACKNOWLEDGEMENT

Great thanks to my advisor Dr. Rafael Sanchez for guiding and encouraging me in this research. Also thanks to Melanie Nelson and Nicholas Williams for their contributions in the laboratory for my data processing. Thanks to the CAPT center, and the help of director Larry Scherrer in training me to use the Wyko Interferometer. Also, thanks to General Motors for providing the materials and inspiration for the research.

## TABLE OF CONTENTS

LIST OF FIGURES.....	x
LIST OF TABLES.....	xii
1. Introduction.....	1
1.1 Motivation.....	1
1.2 Manufacturing background.....	2
1.3 Drawbead Simulator.....	4
1.3.1 Fixed Drawbead.....	4
1.3.2 Roller Drawbead.....	5
2. Prior Work.....	7
2.1 Surface Strain.....	7
2.2 Contact Pressure.....	11
3. Methods of Experimentation and Data Collection.....	12
3.1 Surface Texture Characterization.....	12
3.1.1 Amplitude Parameters.....	12
3.1.2 Volume Parameters.....	13
3.1.3 Spatial Parameters.....	13
3.2 Tested Materials.....	14
3.2.1 Surface Types.....	15

3.3 Material Processing.....	19
3.3.1 DBS Sample Preparation.....	19
3.3.2 DBS Processing.....	19
3.3.3 Uniaxial Tensile Processing.....	22
3.3.4 Pure Bending Moment Processing.....	23
3.4 Optical Interferometry.....	27
4. Results and Discussion.....	29
4.1 DBS Friction Results.....	29
4.2 Roughness Amplitude Results.....	31
4.2.1 Uniaxial Tensile Sa Results.....	31
4.2.1.1 EDT Uniaxial Tensile Roughness Results.....	32
4.2.1.2 MF Uniaxial Tensile Roughness Results.....	34
4.2.1.3. Uniaxial Tensile Interpretation.....	35
4.2.2 Pure Bending Moment Results.....	36
4.2.2.1 EDT Pure Bending Roughness Results.....	36
4.2.2.2 MF Pure Bending Roughness Results.....	41
4.2.2.3 Pure Bending Moment Interpretation.....	41
4.2.3 DBS Results.....	43
4.2.3.1 MF Transverse DBS Results.....	43
4.2.3.2 MF Longitudinal DBS Results.....	45

4.2.3.3 EDT Transverse DBS Results.....46

4.2.3.4 EDT Longitudinal DBS Results.....49

4.3 Plasticity Index Results.....52

5. Summary and Conclusions.....53

Bibliography.....56

LIST OF FIGURES

## Figure

1. Drawbead Schematic and Finished Part.....	3
2. Fixed Bead Drawbead Schematic.....	4
3. DBS by Sanchez.....	5
4. Roller Drawbead Schematic.....	6
5. Processed Sample with Locations Labeled.....	5
6. DBS Sample Strain Histogram.....	10
7. MF Textures in both Longitudinal and Transverse Orientations.....	16
8. EDT Textures in both Transverse and Longitudinal Orientations.....	18
9. Schematic and Photograph of EDM Dissection.....	21
10. Pure Bending Moment Device.....	24
11. Razor Etched Interferometer Image.....	27
12. Wyko NT-2000 Optical Interferometer.....	28
13. Interferometer Objective Lens in Scanning Mode.....	29
14. EDT Uniaxial Tensile Sa Results.....	32
15. MF Uniaxial Tensile Sa Results.....	35
16. MF Transverse Pure Bending Roughness Evolution.....	38
17. MF Longitudinal Pure Bending Roughness Evolution.....	40
18. EDT Transverse Pure Bending Roughness Evolution.....	41
19. MF Transverse Sa Roughness Evolution.....	44



20. MF Longitudinal Sa Roughness Evolution.....46

21. EDT Transverse Sa Roughness Evolution.....47

22. EDT Longitudinal Sa Roughness Evolution.....50

LIST OF TABLES

## Table

I. Friction Table.....	30
II. Sa Values vs. Tensile Strain.....	33
III. Sample Thickness Changes During Pure Bending Sequence.....	39
IV. Plasticity Index for Uncontacted 3B.....	53

## **1. Introduction**

### **1.1 Motivation**

The continued improvement of sheet metal forming requires careful analysis of the surface topography of the sheet metal. The characterization of the surface texture of aluminum alloy sheets is an important parameter influencing formability, friction, and painted appearance for the forming of automotive parts [1]. This characterization is especially important as new surface textures and patterns are introduced. electro discharge textures (EDT) are credited with improving painting and formability and their use is becoming more extensive in Europe[1,2], while traditional mill finish (MF) textures remain popular in North America. While the factory surface finish qualities for these sheets are well known, surface roughness changes affected by forming practices are also of great importance in manufacturing and are of primary interest in this study.

The introduction of non-contact 3d optical interferometer technology allows defining surface parameters to extents not allowed with conventional 2d interferometer techniques. In their studies of sheet metal surfaces, M. Pfestorf et al [3] showed the significant advantages offered by 3D instruments. Optical interferometry is particularly useful for studying contact and friction

phenomena and investigating changes due to the complex interactions with the tooling, lubricants and sheet metal. An extensive presentation of characterization techniques and their applications can be found in [4]. In this study, 3D non contact interferometry is used to measure changes in texture for aluminum alloy sheet under plane strain cyclic bending with stretching and compressing. These modes of deformation are predominant in the forming of automotive parts, and are simulated in this study by the passage of the sheet through cylindrical drawbeads. Other tests, such as the Pure Bending Test, and the Tensile Test, were performed in order to provide fundamental data important to the understanding of the cyclic bending with tension case.

## **1.2 Manufacturing Background**

Controlling the flow of material into die cavities during stamping and forming operations is important for controlling overfeeding of the sheet, wrinkling, and material thinning. This control can be accomplished with the use of blank holders that use friction, or a combination of friction and deformation. In many cases, friction from flat clamping binders is not sufficient to control the flow of the material[5]. In these cases, a drawbead is used (figure 1.).

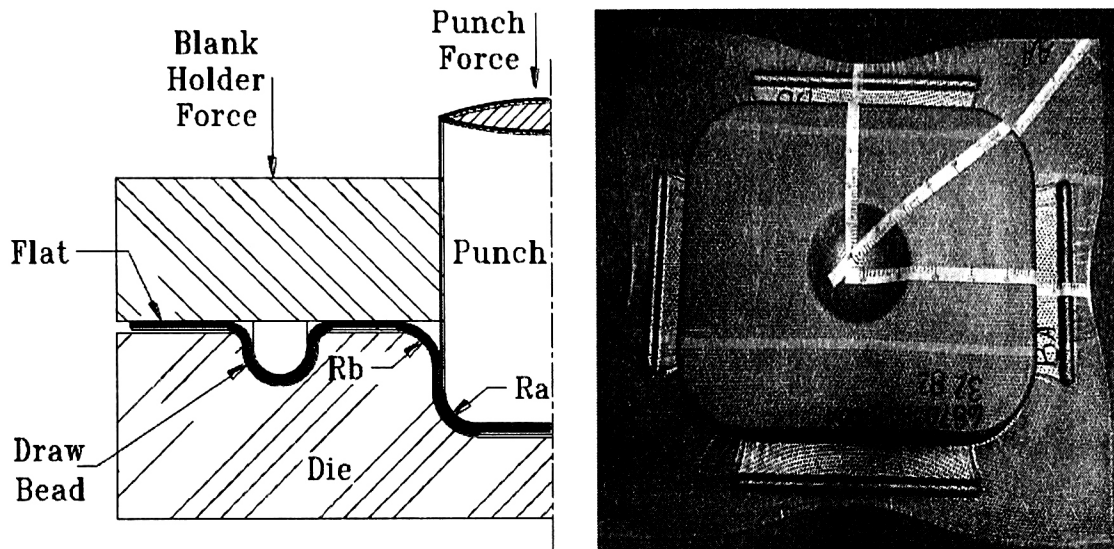


**Figure 1. Drawbead Schematic and Finished Part**

Drawbeads provide the material with back-tension due to both friction and deformation mechanisms. The contribution to back-tension from the force required to deform the material around the drawbead is several times greater than the force of friction imparted by the drawbead. This gives the benefit of smaller blank holder forces, reduced contact pressure, more consistency and reduced friction on the part during forming operations verses entirely friction-based flat blank holder surfaces.

### 1.3 Drawbead Simulator

#### 1.3.1 Fixed Drawbead

The drawbead forming process is replicated using a Drawbead Simulator (DBS) patterned after H. Nine [5]. The sheet metal is pulled at constant rate between three fixed cylindrical pins. While the pins can be positioned with axes non-coplanar, most manufacturing conditions as well as this study are conducted with axes aligned along the same plane. Figure 2 shows a schematic of a three-pin, circular drawbead.

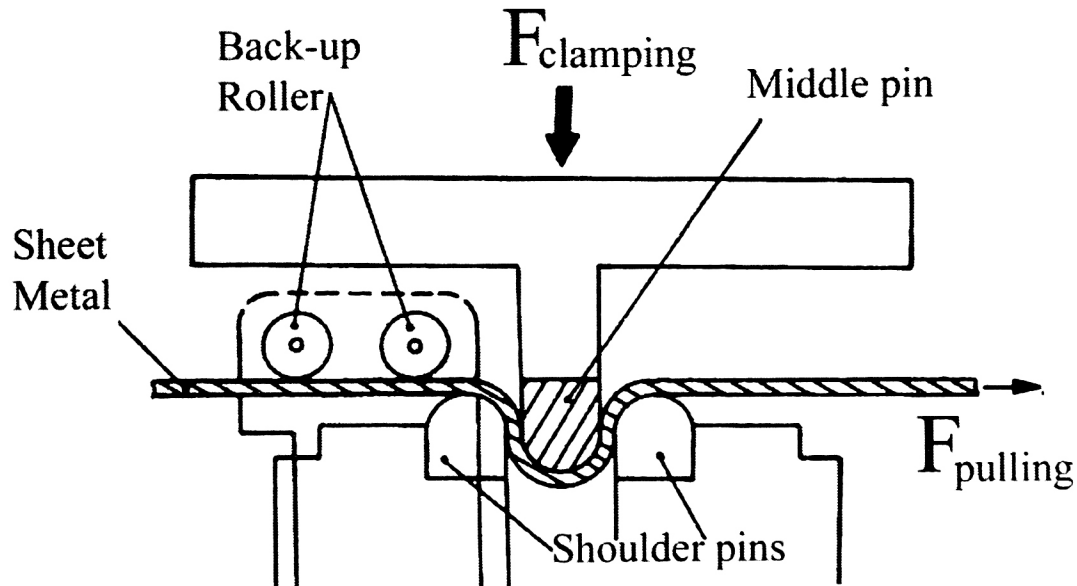


**Figure 2. Fixed Bead Drawbead Schematic**

A DBS designed and fabricated by Sanchez was the device utilized for this study(Figure 3.).

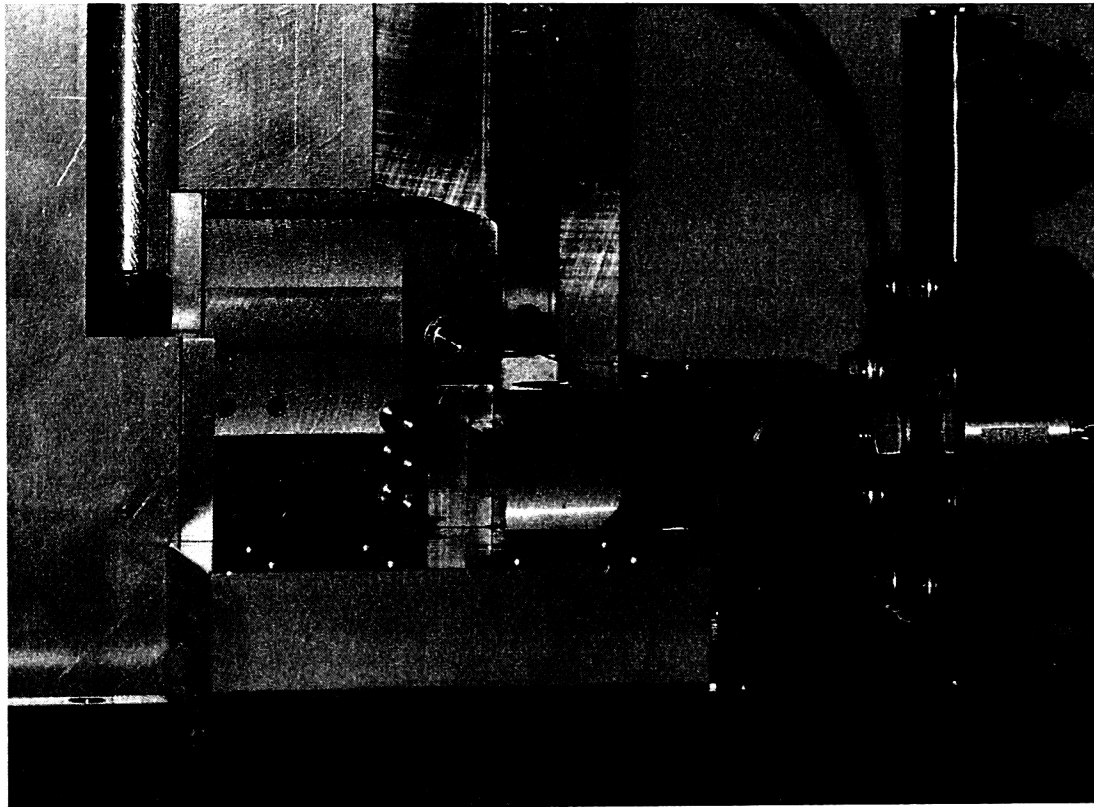


**Figure 3. DBS by Sanchez**

### **1.3.2 Roller Drawbead**

As mentioned earlier, most of the force required to draw the sheet through the DBS is used to deform the material, however the force due to friction is not insignificant. Substituting the fixed drawbeads for rolling drawbeads, the beads are allowed to roll freely with the material (Figure 4.). As the

coefficient of friction for the ball bearings supporting the roller beads is on the order of .002, friction can be considered negligible for this condition.

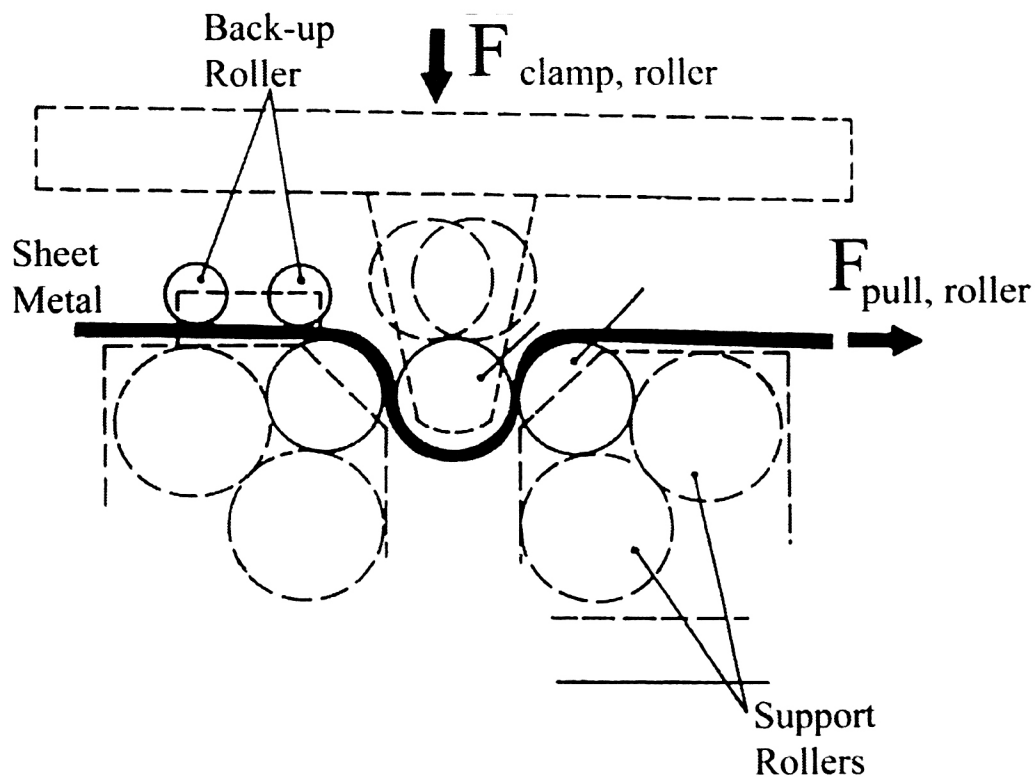


**Figure 4. Roller Drawbead Schematic**

The forces are recorded during the drawing process and the material is tested using both the fixed and roller drawbeads. The pulling and clamping forces are recorded by load cells on the test fixture. The coefficient of friction is determined using the following equation (1)[5].



$$\mu = \frac{1}{\pi} \frac{F_{Pull, Fix} - F_{Pull, Roller}}{F_{Clamp, Fix}} \quad (1)$$

## 2. Prior Work

### 2.1 Surface Strain

Surface straining is one of the two primary mechanisms for affecting surface texture. The DBS process is unique in deforming the sheet under cyclic plastic plane strain. Each test sample is strained in three reversing cycles. The total accumulated strain (the summation of the absolute value of all cumulative strains) at the sheet surface is over 30%(see Figure 5) for typical DBS samples. Resultant strains in the most strained locations can be as much as 20%. The net strain upon exit from the fixed pins depends on friction, but is typically 10%, and approximately the same for both sides. Five locations (Figure 5) were identified as the most significant to our study. The evolution of the surface roughness on the outer layers was investigated in those five positions, on both the concave and convex sides.

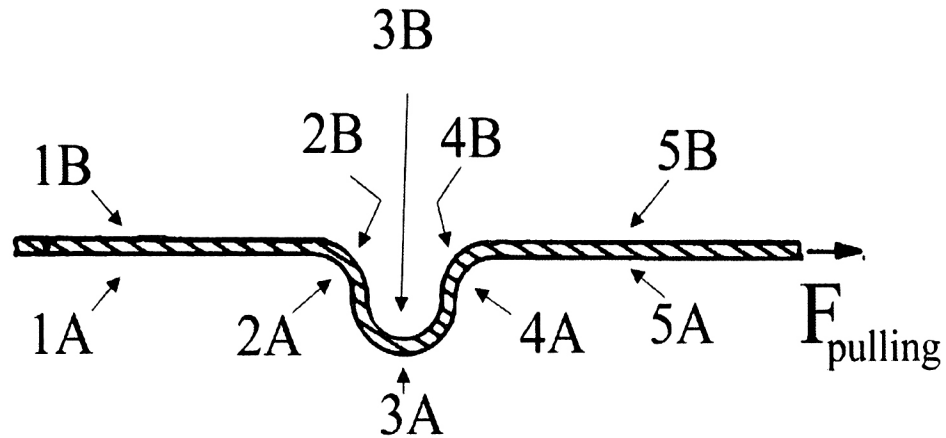


**Figure 5. Processed Sample with Locations Labeled**

In the discussion that follows, it is important to note that the pulling force (the resultant force pulling the sheet through the pins) increases from zero at the inlet to a maximum at the outlet. This implies that the amount of stretching superimposed to bending is different for each pin. Upon entering the DBS, side A is subjected to a compressive strain typically around 9% (region 2) as it bends to conform to the first pin. While side A is concave, and under compressive strains, side B is subjected to tensile strains of similar magnitude to side A. At location 2, the material has bent to contact with the first drawbead pin. The sheet has undergone bending plastic deformation. Since the inlet force is zero, the amount of net pulling force was not significant at this location. This is evidenced by the similar strains on both compressive and

tensile sides seen in Figure 5. During the change in curvature that occurs in between the first and second pins of the drawbead(region 3), the curvature of the sheet is completely reversed within a gap between pins equal to only 0.003 inches plus sheet thickness. The material experiences high strain rates as the sheet passes it inflexion point. Strain rates two orders of magnitude larger than standard uniaxial tensile testing are normal. Nevertheless, aluminum sheets are not strain rate dependent and are unaffected by this rapid curvature change. During this reversal from pin1(location 2) to middle pin (location 3), side A goes from compressive straining to tensile straining, a total change of around 16%. Side B undergoes an opposite, but similar straining mechanism. The net compressive strain on side B at location 3 is smaller than that for side A at location 2, because of the additional effect of the tensile pulling force acting on the cross section. In between the second and the third pin, the sheet undergoes another full reversal as it conforms to the curvature of the third pin (region 4). At this location, side A is on the compressive side, however, the compressive strains are not large. The pulling tension becomes significant at this location and significantly reduces the amount of compressive straining (to about 4% for the case shown in Figure 6.)[7]. The neutral axis has shifted closer to the compressive outer fiber because of this superimposed pulling tension. Upon exiting the DBS at region 5, the sheet is unbent. Strains in side

A become tensile, while those in side B are reduced upon unbending. The net resultant strain (around 9%) are close for both sides, but not equal. Strains at side B remain slightly higher, as the sheet was not unbent past its point of inflection. This results on a noticeable final curvature in section 5 typical of aluminum samples.

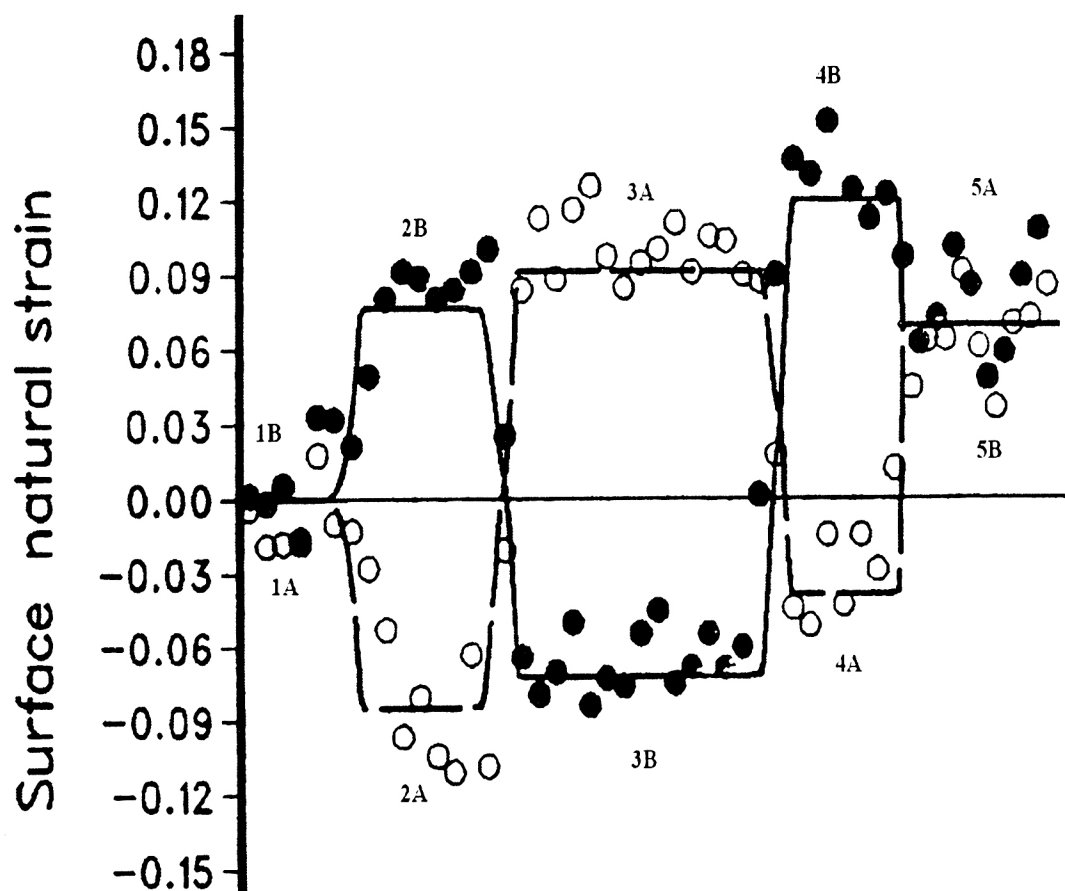


**Figure 6. DBS Sample Strain Histogram**

## **2.2 Contact Pressure**

The contact pressure on the sheet is a function of two phenomena. Describing the first, the sheet wraps around the respective drawbead pins in an arc described by the term sliding angle. The net tensile force at the end of this sliding angle is resolved by the effect of friction caused by the contact pressure against the sheet. For the frictionless case, the pulling tension does not increase through this sliding angle, as the sheet rolls along with the drawbead pin. For the friction case, the tension increases, and thus the contact pressure increases. Because the thickness of the sheet is significant compared to the radius of the drawbead, describing the contact pressure as resolved entirely by the net tensile loads exerted on the sheet following a membrane model is not adequate. As the sheet reverses in curvature at the beginning and ends of the sliding angle, there is a large transverse shear force that must be supported by the pin to execute the bending or unbending. This results in a spike in the contact pressure that represents the most severe contact pressure experienced by the pin[7]. While the analytical model developed by Sanchez does determine the shear forces present on pin entrance and exit, further experimental studies are necessary to assess the actual size of the contact areas for those localized shear effects.

### **3. Methods of Experimentation and Data Collection**

The surfaces parameters under investigation are the 3-Dimensional Roughness average (Sa), normalized volume, RMS roughness (Rq), and various spatial parameters. The roughness average and volume parameters were primary indicators of the effect of the DBS on the sheet surface features and are the parameters discussed here. Other spatial parameters are used to predict the changes on the surface due to contact forces.

#### **3.1 Surface Texture Characterization**

##### **3.1.1 Amplitude Parameters**

There are a myriad of surface texture parameters that can be used to characterize a surface. Amplitude parameters provide information relating to the height differences in surface valleys and asperities. Sa or surface roughness arithmetic average is a common amplitude parameter used in manufacturing (Equation 2.).

$$Sa = \frac{1}{n} \sum_{i=1}^n |Y_i| \quad (2)$$

The variable  $Y$  is the distance of a surface point from a plane defined as the mean of the surface.

RMS or RQ roughness is a measure of the standard deviation of the surface. High asperities and Valleys are given greater weight than in  $S_a$  calculations(Equation 3.). This parameter is important in performing contact analysis.

$$Rq = \sqrt{\frac{1}{n} \sum_{i=1}^n Y_i^2} \quad (3)$$

### 3.1.2 Volume Parameters

Surface volume data defines the volume of empty space between the lowest valley of the surface to the top of the highest peak. This parameter is evaluated in this study because it is used in evaluating mean lubricant film thickness, deformation of local maxima, and lubricant containment.

### 3.1.3 Spatial Parameters

Amplitude parameters do not supply any information related to the spatial characteristics of features. Two surfaces represented by sine waves can have

equal amplitudes and  $S_a$  values but vastly different shapes given by different frequencies. Surface deformation and friction characteristics are dependent not only on amplitude parameters, but also spatial-dependent parameters such as asperity radius and asperity frequency.  $N_0$  is the number of zero crossings per unit length.  $N_p$  is the number of local maxima per unit length, where a local maxima is defined as any point where the adjacent points are lower.  $R_p$  is asperity tip radius.

### **3.2 Tested Materials**

The material under investigation for this study is 6000 series cold-rolled sheet aluminum. Although the material of choice for automotive application is sheet steel (lower cost), aluminum is increasingly considered a material of choice for automotive applications due to its more advantageous weight and strength characteristics. Aluminum is strain rate insensitive, but it is more prone to surface damage such as scoring and galling. Also, while steel is more isotropic, the mechanical properties of aluminum show dependence on the direction of the grain and its behavior is more orthotropic.



### **3.2.1 Surface Types**

The two surface types under investigation are created with two different methods. Mill Finish (MF) textures are the standard rolled surfaces created by the rolling process. The rollers are tangentially ground, imprinting directional grain effects on the sheet. They have relatively low roughness, but exhibit different frictional properties along different directions. The roughness inherent to the sheet is a byproduct of the elongation and deformation of the grain structure under the finish roller. Figure 7 shows a 3D surface roughness texture typical of mill finish. The anisotropic roughness is noted along the longitudinal and the transverse directions.

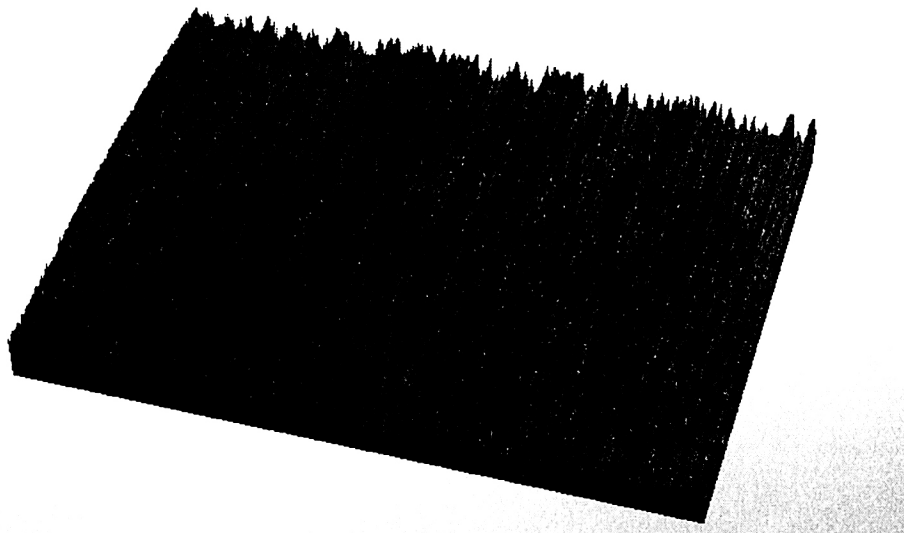
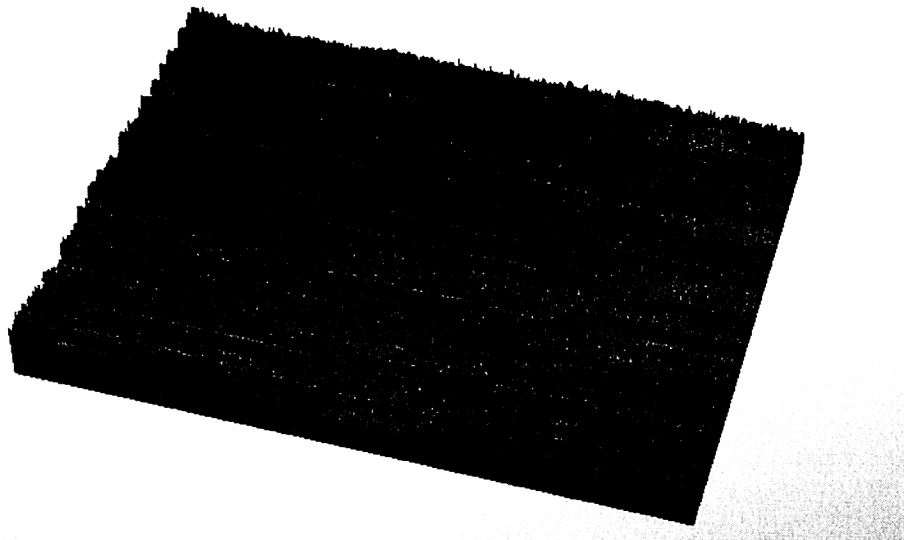


**Figure 7. MF Textures in Both Longitudinal and Transverse Orientations**

Electro-Discharge Textures (EDT) are created by rolling the sheet using a special roller that has been textured by an electrodischarge process. The texture of the drum is impressed onto the rolled sheet. EDT textures are more

expensive to produce than MF textures. In this study, EDT surfaces will be analyzed in both the longitudinal and transverse directions. EDT textures (Figure 8) do not show a preferential pattern with direction.

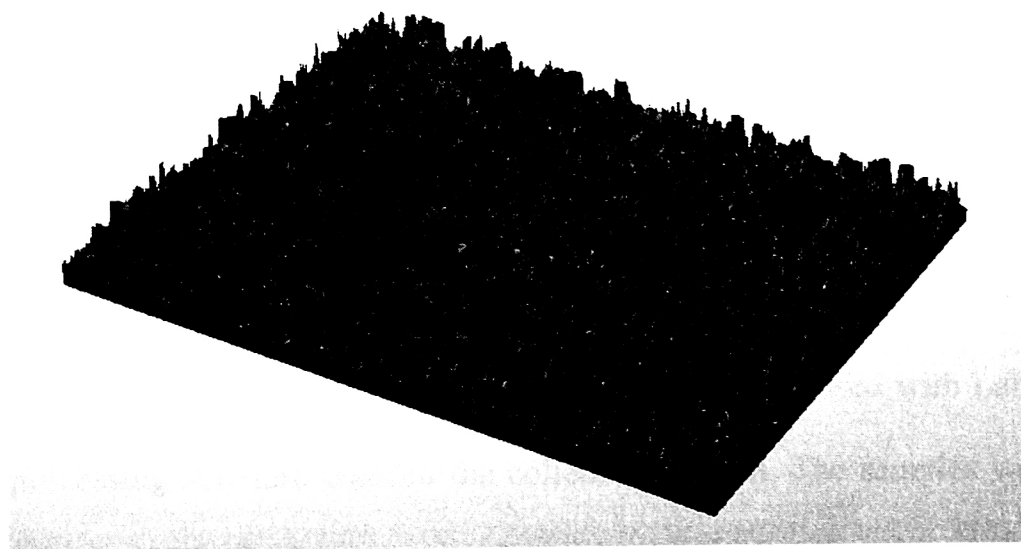
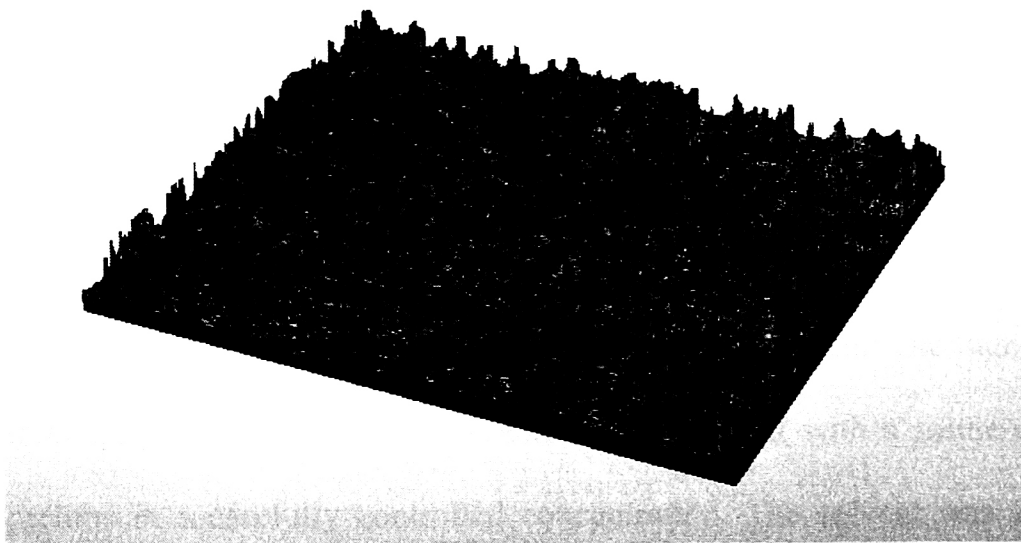


**Figure 8. EDT Textures in Both Transverse and Longitudinal Orientations.**

### **3.3 Material Processing**

#### **3.3.1 DBS Sample Preparation**

DBS samples of dimensions 2"x16"x sheet thickness were cut from a large blank with a power shear, and the edges were de-burred with a hand tool. These samples were scrubbed with a combination of isopropyl alcohol and P-xylene to remove all debris and packing grease. The samples were immersed in a bath of Enviro-Tech N-solv solvent with a solute of MP404 prelube in a carefully controlled concentration. The solvent was allowed to dry leaving a film of oil weighing 1 gram per square meter. The proper mass application of oil was verified using a precision scale.

#### **3.3.2 DBS Processing**

Once the samples are cut, cleaned, and lubricated, they were subjected to testing in the DBS. A PDAQ data acquisition system used with Labview data processing software enabled the collection of data. The samples were loaded into the DBS, the bottom was clamped using hydraulic grips, and the center drawbead was moved into place with a hydraulic ram, forcing the part to conform to the contours of the drawbeads. A large power screw was actuated electronically and the hydraulic grips pulled the sample through the beads at a rate of 85 mm/s (200 ipm). The pulling force and the clamping force were

recorded during the entirety of the process. An initial transient condition is present due to the inertia of the device components and the static friction that is overcome at the start of the process. Pulling and clamping data were collected around mid-stroke, where the data typically exhibit a plateau. Data from the plateau are used in the friction and load calculations. The sample is carefully removed from the apparatus and packaged in order to prevent surface damage. The sample is then dissected into five small sections using an EDM wire cutting machine (Figure 9), allowing the interferometer lens access to the areas of interest. This process was repeated for all samples using both the roller drawbeads and the fixed drawbeads.

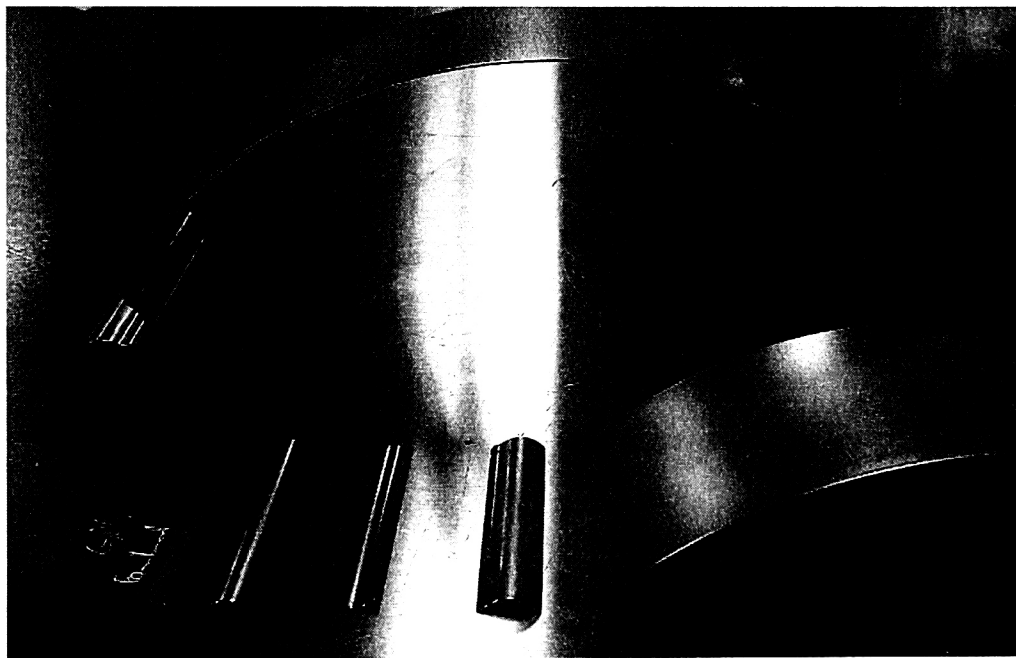
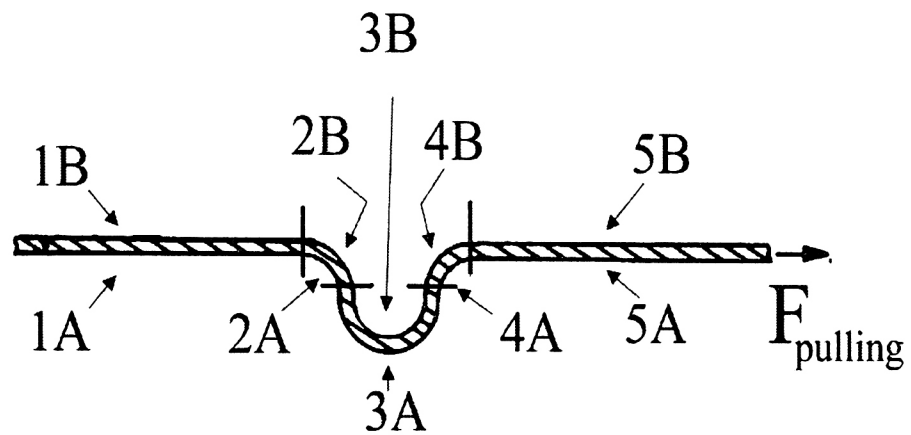


**Figure 9. Schematic and Photograph of EDM Dissection**

The outer layer for side A can be seen to evolve from flat to concave (location 2) to convex (location 3) to concave (location 4) to (approximately) flat at the exit (location 5).

Correspondingly, the outer layer of side B becomes convex at location 2, concave at 3, convex at 4 and unbent to ~flat at 5.

It is noted that the contact sections at which friction is operative are given by the concave outer layers, locations 2 and 4 side A, and location 3, side B. At those locations, the resulting amount of compressive straining depends on the contribution of the amount of pulling tension at the location. The resulting Sa roughness values may depend on this resultant straining, added to peak flattening resulting from sheet and tool contact.

In an effort to isolate the combined effect described, two additional tests were included in the surface roughness tests: the uniaxial tension test, and the pure bending moment test.

### **3.3.3 Uniaxial Tensile Processing**

Uniaxial samples were processed on an Instron test fixture. These samples were razor etched perpendicular to the direction of tension for tracking strain data after processing. The samples were strained monotonically. It should be noted that the strains from the tensile test are uniaxial, while the strains from the DBS are plane strain, with approximately zero strain along the width (since the sample width remains constant). The uniaxial tension test follows



the ASTM E8 standard for sheet metal. It is universally used and no further details are given here.

#### **3.3.4 Pure Bending Moment Processing**

The pure bending moment device was developed by Sanchez to investigate plane strain pure bending, Bauschinger Effect and springback phenomena. It is noted that the plastic strains from this test are plain strain, as are the strains from the DBS tests. A major difference to the DBS is the zero pulling tension under pure bending. Figure 10 shows the working mechanisms of this device.

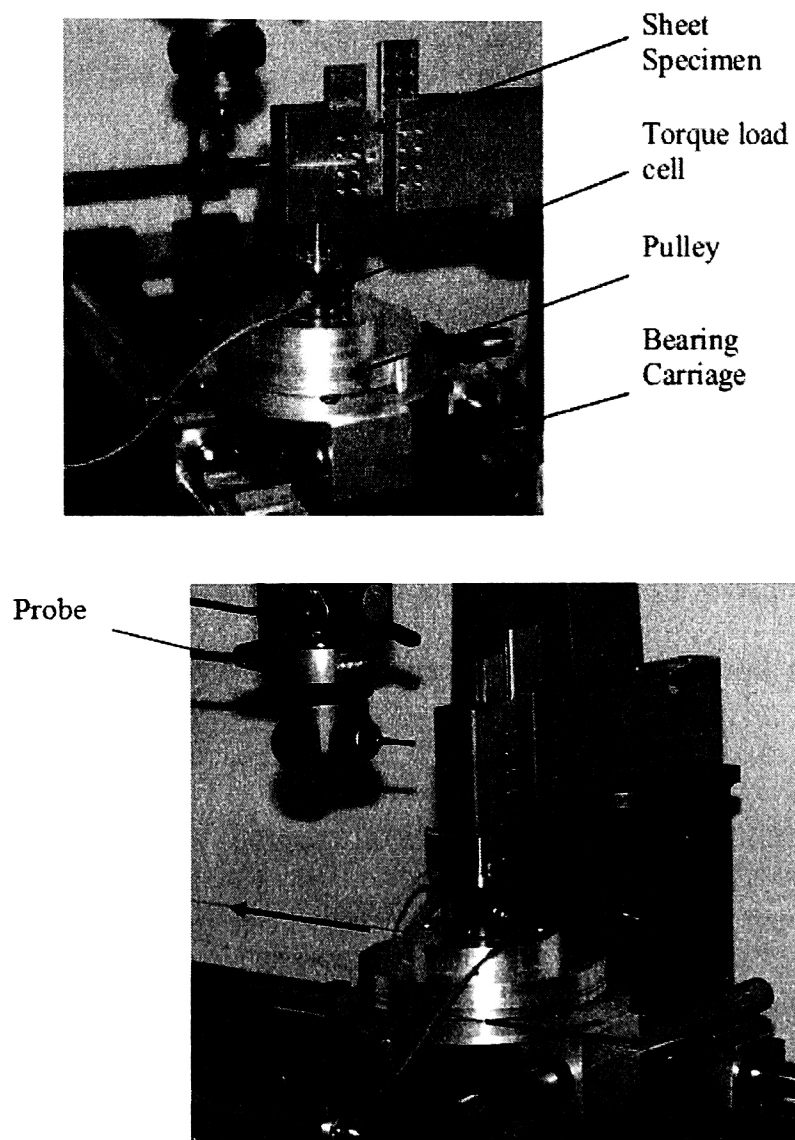


**Figure 10. Pure Bending Moment Device**

The sheet is held between two clamps. One clamp is mounted to a rigid frame and the other is mounted to a moving mechanism consisting of a load cell, a pulley and a moving carriage. The pulley is supported by a bearing and rotates freely on the moving carriage. The carriage is supported on linear bearings and the pulley can rotate and translate in the horizontal plane with minimum friction. Weights hanging on cords (not shown) apply the couple shown by the arrows in Figure 10. The couple is opposed by the resistance of the sheet to bend and it is monitored by the torque load cell. The load is removed during unloading. Reverse loading is applied by wrapping the strings on the opposite direction, inverting the direction of the load applied to the pulley.

Before processing in the pure bending moment device, the samples were cut to 2"x2" size and marked with a razor etched grid in the center of the bending area (Figure 11). This grid was used to track the strain of the outer fibers of the material. The use of strain gauges on pure bending moment samples is difficult and laborious due to strain gage requirements for large deformations. To achieve strains similar to that of the DBS, the sample has to be bent in a very narrow region, and the maximum strains either require plastic strain gages that are difficult to mount and require high oven

temperatures and large curing times. Furthermore, strain gages must be discarded under reverse bending due to hardening effects.

The device was carefully loaded in a two person team. Weights are slowly added to both sides of the machine in tandem to ensure the only load on the sample is a bending moment. Weights are added until the sample reaches a curvature of the same radius as the drawbeads on the DBS. Achieving levels of strain similar to that of the DBS was the goal in order to investigate the effect of tensile and compressive strain in the absence of contact forces. The part was then carefully removed from the device, scanned in the interferometer, and returned to the device to perform a reversal of the bending cycle that was executed prior. A total of three bends and rebends were performed, replicating the cyclical bending of the DBS machine. Surface data was also captured for strains between the two bending reversals (flat surface between bending – reverse bending).

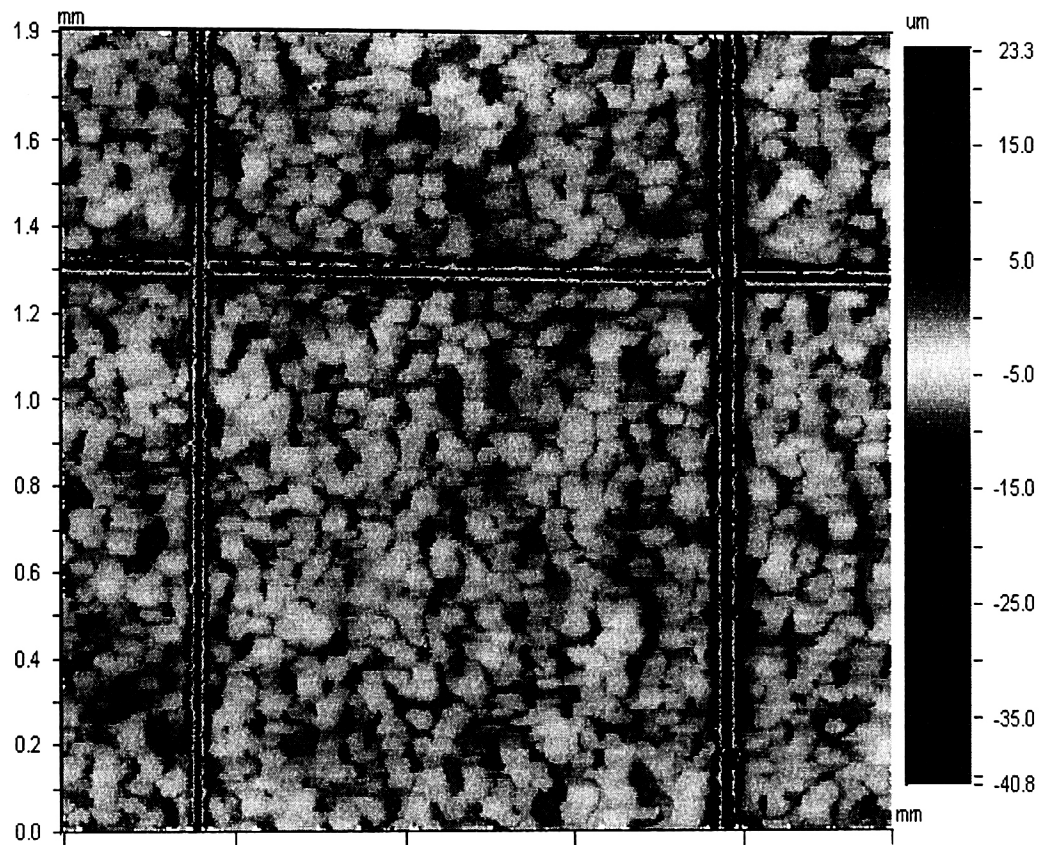


**Figure 11. Razor Etched Interferometer Image**

### **3.4 Optical Interferometry**

For this study a Wyko NT-2000 optical interferometer (Figure 12.) was used for 3d surface data collection. The interferometer was operated in VSI (vertical scanning interferometry) mode. The scan area was 2.432mm by 1.852 mm with a lateral resolution of 3.31  $\mu\text{m}$  and a vertical resolution of .1

nm. This resolution was more than adequate to capture the features of the aluminum sheet.

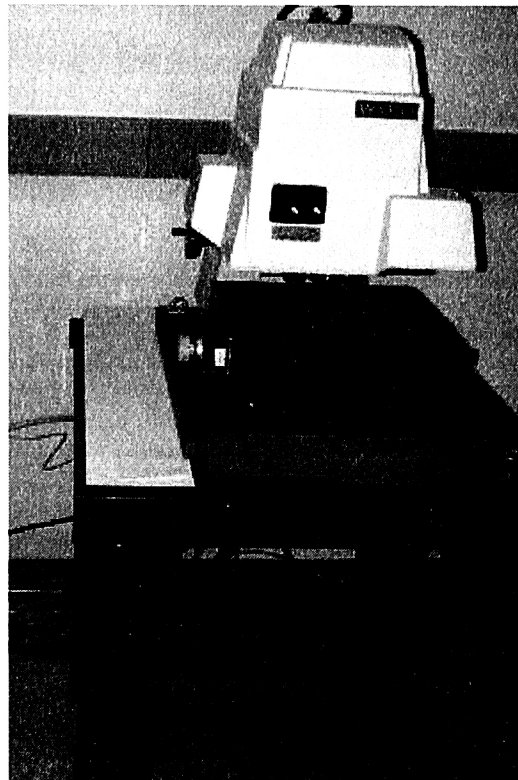


**Figure 12. Wyko NT-2000 Optical Interferometer**

To scan the data, the sample was placed squarely under the objective lens (Figure 13). The curved samples were positioned such that the scan occurred at the center of their arc. The interferometer scans from the top down, capturing the highest features first and then scanning down towards the lowest points of the surface. The vertical scanning distance was adjusted from 25  $\mu\text{m}$  for flat surfaces to up to 180  $\mu\text{m}$  for curved sections.

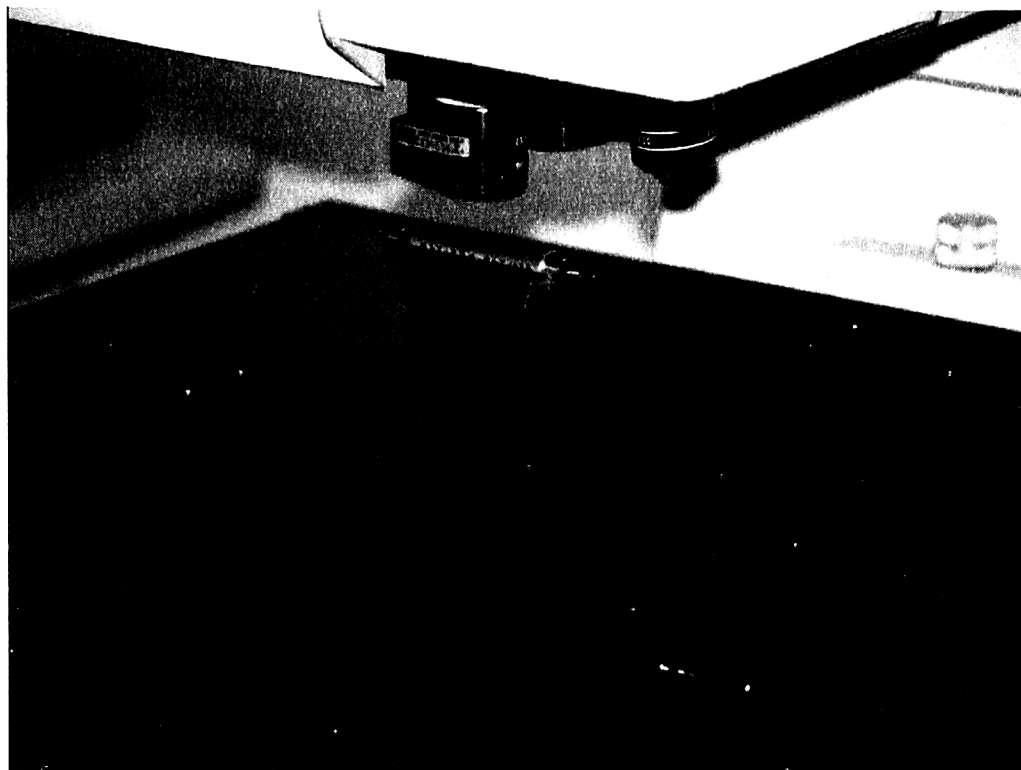


**Figure 13. Interferometer Objective Lens in Scanning Mode**

The result of the scan is an optical file representing the surface of the samples.

## **4. Results and Discussion**

### **4.1. DBS friction results**

The friction results gathered by the DBS test device are created using samples cut from the same blank, and are created using averages from at least ten samples. This ensures the roller DBS samples and the fixed bead DBS

samples will possess the same mechanical properties and surface texture. The friction and load results are as follows (Table I)

Table I. Friction results for EDT samples and MF for two suppliers

Material	Surface Finish	Rolling Direction	Roller Force	DBS Friction
			N	Coefficient
AA6022	Mill Finish	Longitudinal	3273	0.078
	Mill Finish	Transverse	3120	0.048
GMW15192	Mill Finish	Longitudinal	3212	0.088
	Mill Finish	Transverse	3078	0.031
GMW15192	EDT	Longitudinal	3114	0.122
	EDT	Transverse	2944	0.115

Although for these materials Mill Finish texture has the lowest friction characteristics for both longitudinal and transverse directions verses the EDT samples, this is not necessarily more desirable. EDT textures offer close to isotropic friction, with very small difference between longitudinal and transverse directions. MF instead, has significant differences on friction along the longitudinal and transverse directions. The trend of reduced friction in the transverse direction verses the longitudinal direction has also been reported in other sliding friction studies. It is believed that transverse roughness characteristics promotes larger film thicknesses than longitudinal surfaces in similar conditions[6]. It is interesting to note that the tensile pulling forces



reported for the Roller in Table I , results on stresses around 10 000 psi, which are significantly smaller than the yield of the material. The combined bending and stretching mechanism allows for the plastic deformation under DBS testing.

## **4.2 Roughness Amplitude Results**

Roughness average Sa is a common measure of surface roughness in the automotive industry. The effects of the DBS process are evident in the study of the evolution of the surface Sa roughness as it travels through the DBS. To develop a fundamental understanding of the effects of material processing on the samples, the results from the simpler uniaxial tension and pure bending moment tests are presented before the DBS results

### **4.2.1 Uniaxial Tensile Sa Results**

The uniaxial tensile test is a common test used to evaluate the strength and hardening properties of material. Our material was strained in two steps. The material was strained to around 10% elongation, since most of our testing is around this magnitude of strain. One side of the tensile test sample was selected and scanned for roughness data. The test sample was then replaced in

the uniaxial tester and strained to failure. The at-failure samples are then scanned for roughness data.

**4.2.1.1 EDT Uniaxial Tensile Roughness Results**

The results for both longitudinal and transverse orientation EDT samples are plotted in Figure 14.

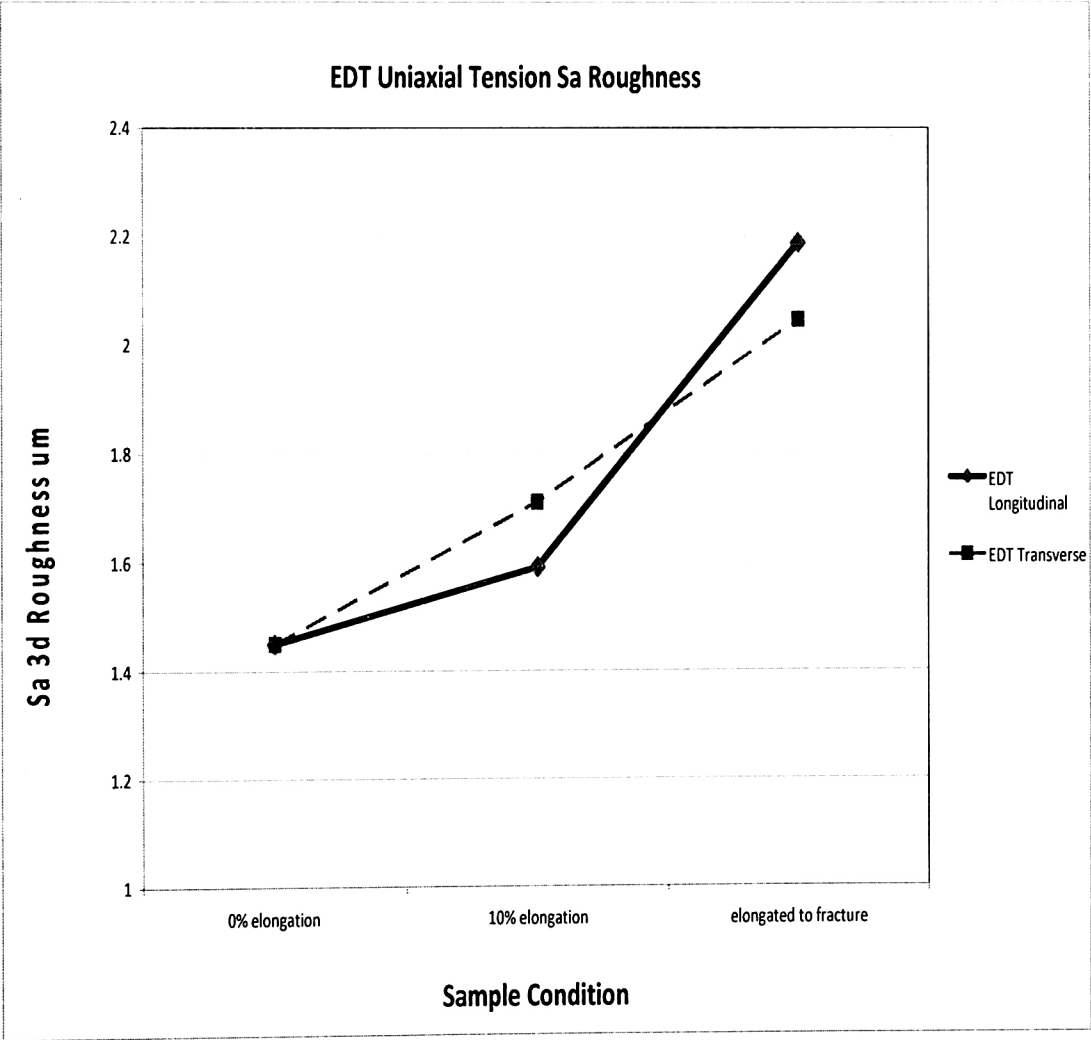


**Figure 14. EDT Uniaxial Tensile Sa Results**

It is observed that the evolution of the surface roughness in the tensile test was linear with tensile strain for the EDT along the transverse direction (T) , and non-linear along the longitudinal direction (L). Sa is smaller for the longitudinal sample than for the transverse sample at 10% strain. However, the trend reverses for the L sample at fracture. It should be noted that the longitudinal sample fractured at 28.3% elongation where the transverse sample fractured at 22.25% elongation. The increase in roughness for the longitudinal sample may be due to reaching larger strains. Of interest here are the Sa values around 10% strain (Table II).

Table II. Sa values vs. Tensile Strains

Condition	Tensile Strain	Sa ( $\mu\text{m}$ )
EDT L	10%	1.56
EDT T	10%	1.47
MF L	10%	.77
MF T	10%	.80
EDT L	Fracture at 28.3%	2.1425
EDT T	Fracture at 22.25%	1.8075
MF L	Fracture at 28.2%	1.415
MF T	Fracture at 28.75%	1.57

Although the effect of tensile strain on Sa is considerable at fracture (around 40% and 50% at T and L, respectively), it is much less pronounced at 10% strains, with (10% along L and 18 % along T)

#### **4.2.1.2 MF Uniaxial Tensile Roughness Results**

The results for the MF samples exhibit similar monotonic increases in surface roughness under tensile strains (Figure 15.). The transverse sample achieves a higher roughness than the longitudinal case. However, the difference is small and may be equivalent at 10% strain. The fracture strains are 28.75% for the transverse case and 28.2% for the longitudinal case.

These results show high sensitivity of Sa values to mill finish tensile straining. At fracture, Sa increased from an average of .35  $\mu\text{m}$  to 1.4 -1.6  $\mu\text{m}$  Sa. This represents an Sa increase to tensile strains at fracture of more than 300%. This number compares to 40-50% increase on Sa for the EDT samples.

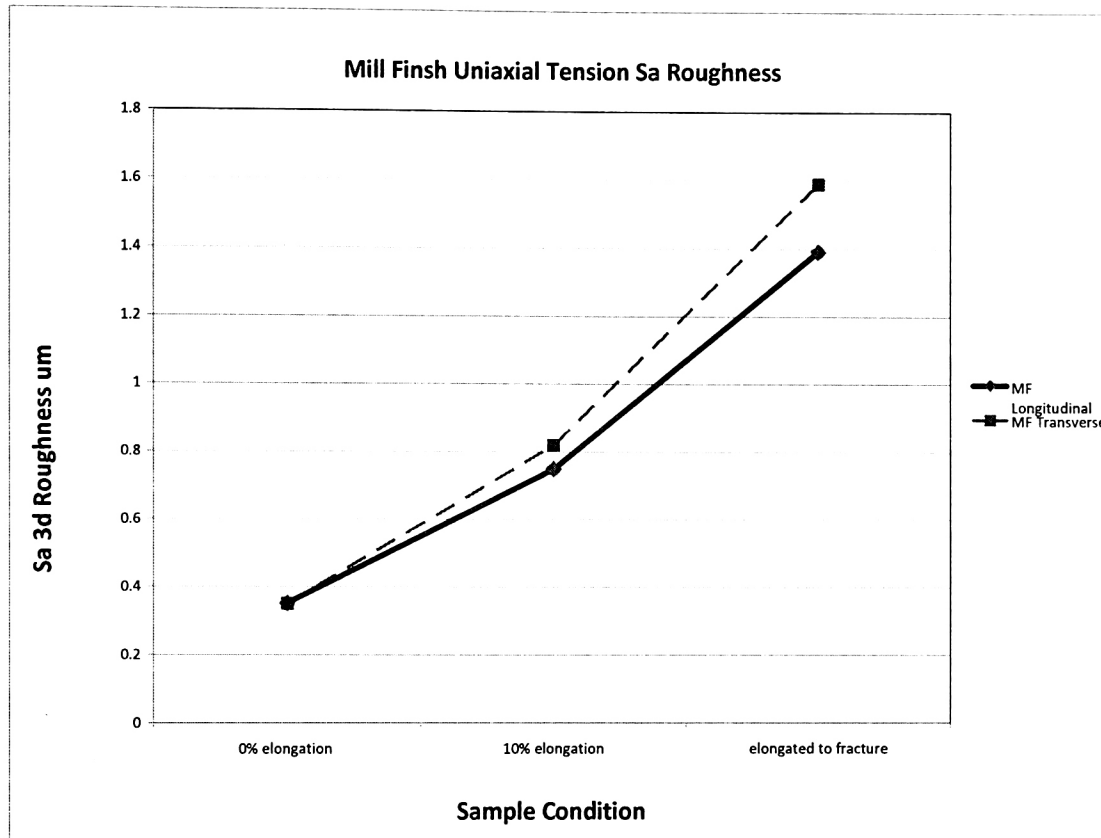


**Figure 15. MF Uniaxial Tensile Sa Results**

#### **4.2.1.3 Uniaxial Tensile Interpretation**

Previous studies indicate that the increase in surface roughness due to intrinsic surface defects occur as a result of surface displacement fields that occur as a result of microstructural dynamics during tensile plastic straining [8,9]. Earlier studies have shown surface roughness to increase linearly during low-strain conditions [10], and to become increasingly non-linear for greater strains [11]. Surface roughness increases linearly and monotonically for tensile strains from 0 to 10%, as shown in Table I.

#### **4.2.2 Pure Bending Moment Results**

The results for the pure bending moment give important insights on the mechanisms influencing surface roughness in the DBS test that the uniaxial test simply cannot give. The pure bending moment device allows the investigation of roughness changes for compressive and tensile strain under cyclic loading. The compressive strains develop as free surfaces, and do not include contact or friction effects. While the literature reports extensive  $S_a$  values in terms of tensile strains, compressive strains on sheet metals are largely missing. In addition, pure bending strains are plane strains, which is also the mode of deformation in DBS testing.

As shown in Table I, DBS friction for MF samples are significantly different for the L and T directions, but close to isotropic for EDT.  $S_a$  evolution under cyclic pure bending was determined for the MF sheets along the longitudinal and the transverse directions, but limited to the transverse direction for the EDT material.

##### **4.2.2.1 MF Pure Bending Roughness Results**

The Pure Bending  $S_a$  values for the MF Transverse texture are shown in Figure 16. Starting from the originally flat sample, the  $S_a$  values for side A and Side B are identical during the first bend in which side A is concave. Bent

from flat,  $S_a$  increased from 0.4 to  $\sim 0.84 \mu\text{m}$  for both sides. This implies that the compressive (concave side) and tensile strains (convex side) had an equivalent influence in  $S_a$ . This is significant, since under tensile strains new surface opens up, and the surface reduces under compression. Upon unbending the  $S_a$  roughness decreases to close the original values for both sides.

Since the tensile strains effects on  $S_a$  under tensile testing are equivalent for the L and T directions, these results correlate well for this first cycle under pure bending. It shows an equivalent  $S_a$  behavior under both tensile and compressive strains.

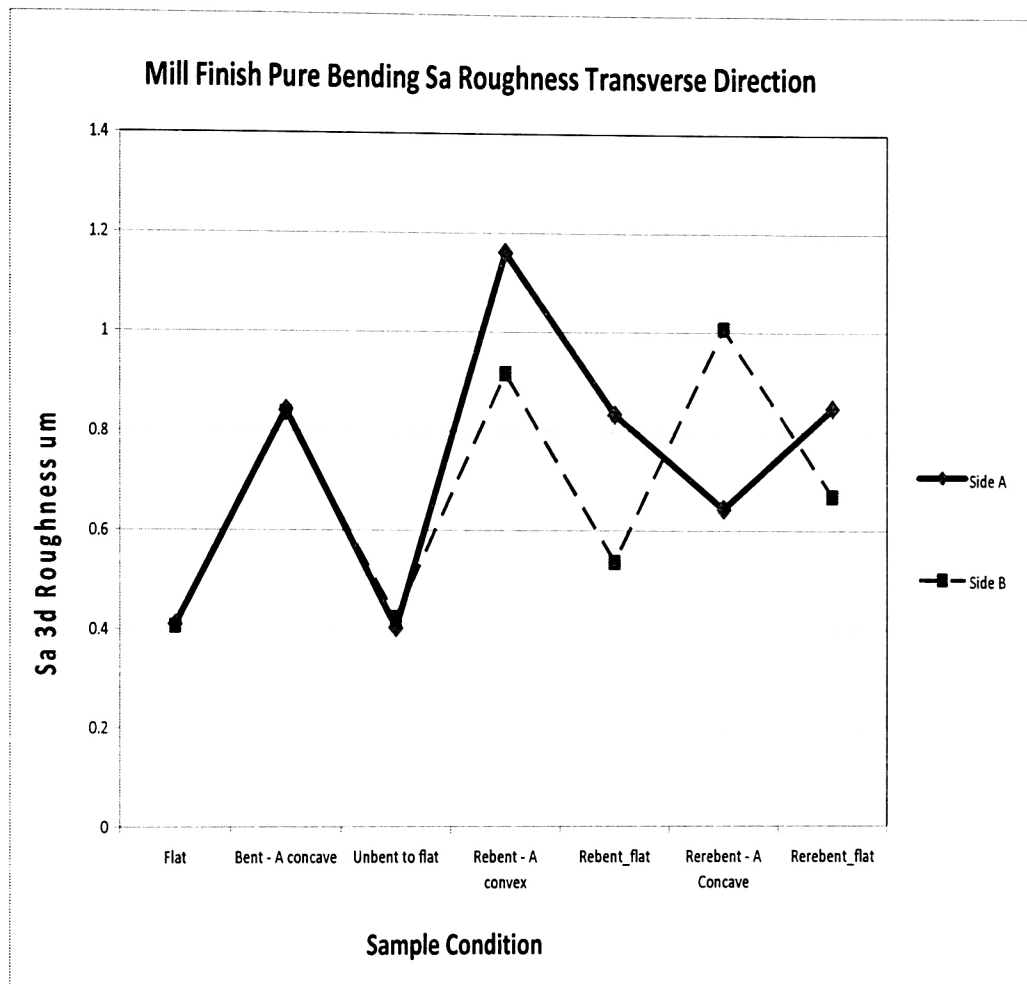


**Figure 16. MF Transverse Pure Bending Roughness Evolution**

The Sa values evolve differently after the first bend-unbend. This behavior depended on which side was bent first. For Side B (convex first) Sa exhibits a regularly increasing pattern during the sequence rebending- flat-second bending-flat. Sa values consistently increased under tensile strains (convex side) and compressive strains (concave side).



The Sa values depart from the pattern above for side A (concave first). When rebent from flat to convex after the first bent, side A is under tensile strains and Sa increased. From convex to flat Sa decreased, but not to the extent anticipated. The difference on Sa values between the two sides becomes significant.

Sa values for side A departs from previous trends when changing from flat to concave for the second time. Under the compressive strains, Sa actually decreased substantially, resulting on the largest Sa difference between the sides. This difference becomes smaller, but still significant, upon the last unbending to flat.

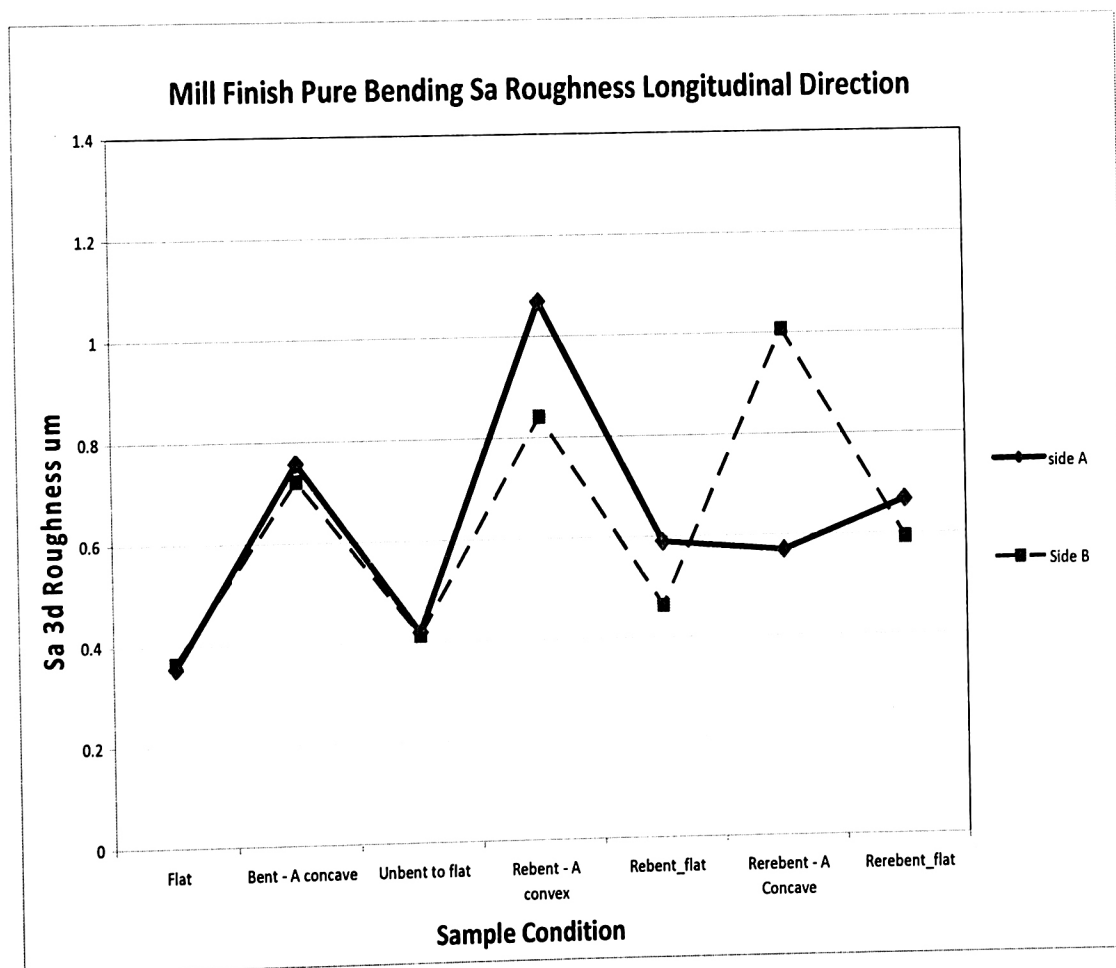
An explanation to this behavior must take into account the changes on sheet thickness during this cyclic bending sequence. The degree of bending is severe, and these thickness changes are not small, as shown in Table III.

Table III. Sample Thickness Changes During Pure Bending Sequence

Sample	Direction	Flat	First bend	Flat	Rebend
Mill Finish	T	0.0386	0.0386	0.03815	0.0378
	L	0.0385	0.0385	0.0382	0.03785
EDT	L	0.0378	0.03775	0.03755	0.03735
	T	0.0378	0.03775	0.0375	0.03715

The change of thickness imposes a net stretching effect on the sample. It is noted that this stretching operates under pure bending. Potential contributions due to out of equilibrium forces, or device misalignment are not present. Furthermore, the forces (weights) used in the Pure Bending test are extremely small (around 6 -7 lbs).

The trends for Sa values described above for MF along T apply directly to Pure Bending Sa values along the longitudinal direction (Figure 17).



**Figure 17. MF Longitudinal Pure Bending Roughness Evolution**

The pattern replicates for all cycles and similar discussions apply. Sa differences between directions mostly occur during the last two bends, when side A goes from flat to second concave. These differences are taken as distinctive to the texture differences between the L and the T directions.

#### 4.2.2.2 EDT Pure Bending Roughness Results

The results for the EDT transverse sample are given in Figure 18.

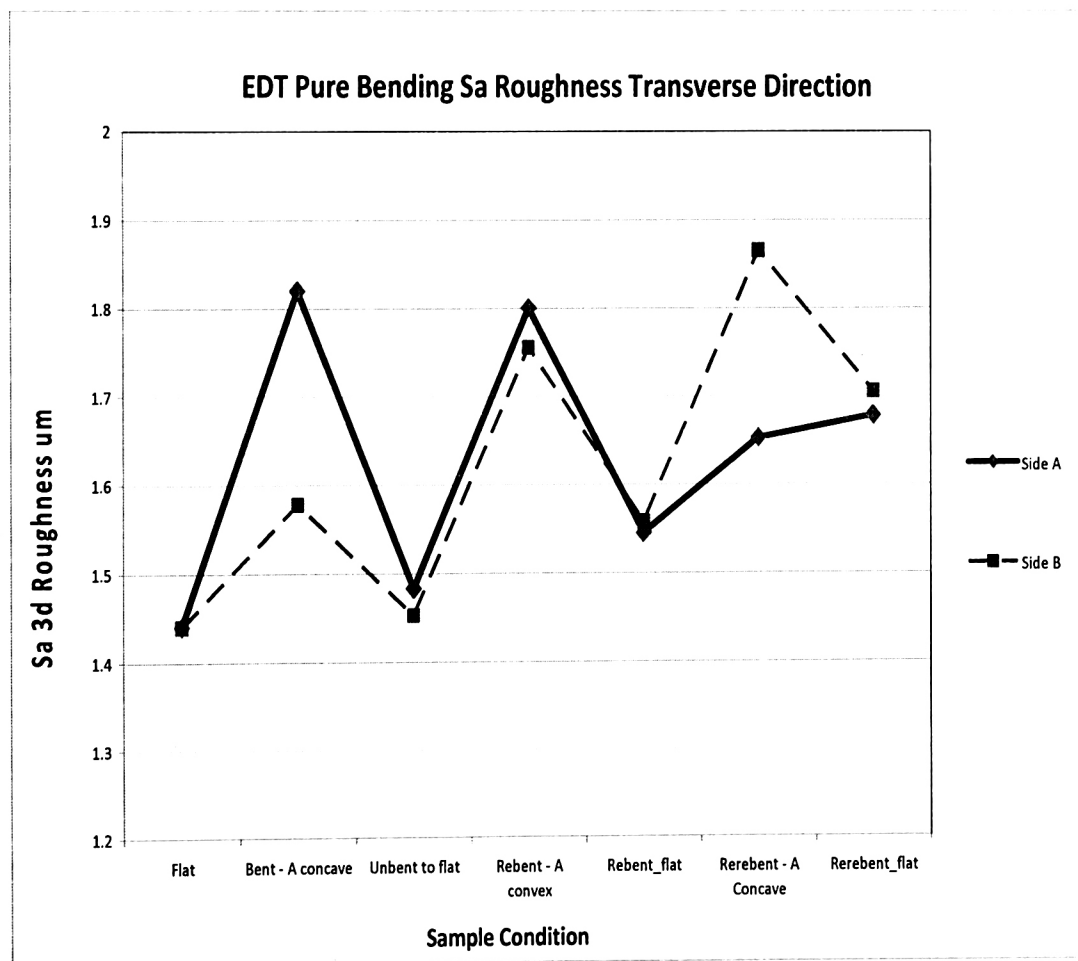


**Figure 18. EDT Transverse Pure Bending Roughness Evolution**

Some general trends show similarities with those shown for the MF samples. For Side B (convex first) Sa exhibits a regularly increasing pattern during the sequence rebending- flat-second bending-flat. Sa values (side B) consistently increased under tensile strains (flat to convex side) and compressive strains (flat to concave side).

EDT Sa values between the first tensile (convex) and compressive (concave) sides were different. Sa values were smaller under tensile strains. These results depart from the MF samples for which both sides had equivalent Sa (Figures 16, 17). This behavior shows as related to the EDT texture, which under Pure Bending the compressive side (concave) becomes rougher at the first bend.

Given the increased pattern for the Sa values for side B, Sides Sa differences decrease as side A goes from flat to convex. Once again, Sa side differences become pronounced at the last flat to second concave. As for the MF samples, this effect is attributed to the stretching mechanism operating under Pure Bending under severe plastic deformation.

It is noted that Sa changes for EDT textures are less pronounced than those for MF texture. Furthermore, as EDT samples start from a Sa value significantly higher (1.45 ) than for MF samples (0.35 ) the percent Sa change

for EDT samples is around 30%, and compares to higher than  $\sim 200\%$  change for MF textures,

### **4.2.3. DBS Results**

#### **4.2.3.1. MF Transverse DBS Results**

The results showing the evolution of  $S_a$  as the sheet slides through the DBS are shown in Figure 19 for the fixed (black) and the roller pins (blue). Solid lines represent side A and dashed lines correspond to side B.

The sheet is bent to the first pin at location 2, with side A concave and side B convex. As the sheet bends, it contacts the pin and exerts contact pressure. However, the back pulling force is zero at the inlet, and the strains are mostly due to bending. The A and B surfaces increase equally in the same manner as the equivalent pure bending operation and they correlate with Pure Bending results given in Figure 15.

The equivalency to pure bending ends with the sample's contact at the second pin in section 3B. The contact pressure is sufficient to flatten the material to starting roughness. The same trend is observed at point 4A, where maximum contact pressure is expected at this location.

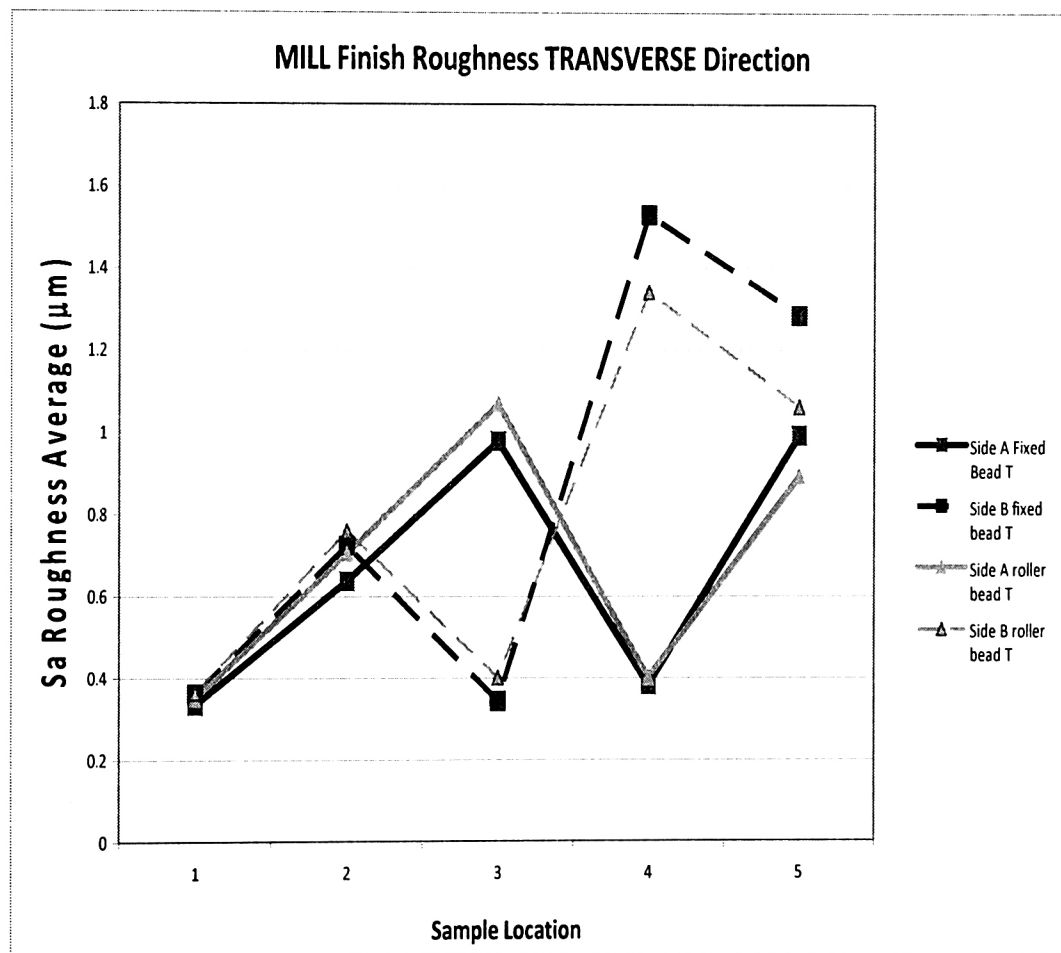
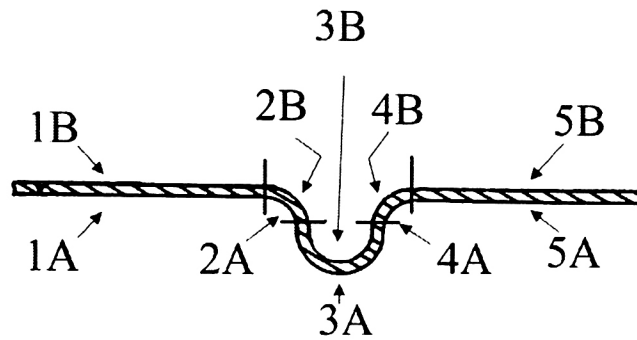


**Figure 19. MF Transverse Sa Roughness Evolution**

The Sa values for the roller device closely follow the results for the MF Transverse up to location 3. This is expected, as the friction coefficient for MF Transverse is very low ( 0.031). Differences are more evident at the exit pin 3 (location 4), and at unbending (location 5). The pulling tension is significantly greater than the roller for the MF sample at those locations.

#### **4.2.3.2. MF Longitudinal DBS Results**

The MF Longitudinal DBS sample showed quite similar results to the MF Transverse sample (Figure 20). The exceptions are the free surface tensile strain (convex side) roughness values, which are significantly lower than those for the transverse sample at locations 4 and 5. Recent studies by Mahmudi and Mehdizadeh showed that increased non-homogeneity in the strain direction of a transverse rolling structure exhibited more pronounced roughening than in the longitudinal direction for tensile straining (materials processing technology citation). This may explain the decreased roughness in tensile locations compared to the transverse MF case despite the higher total load as a result of increased friction and orthotropic hardness.

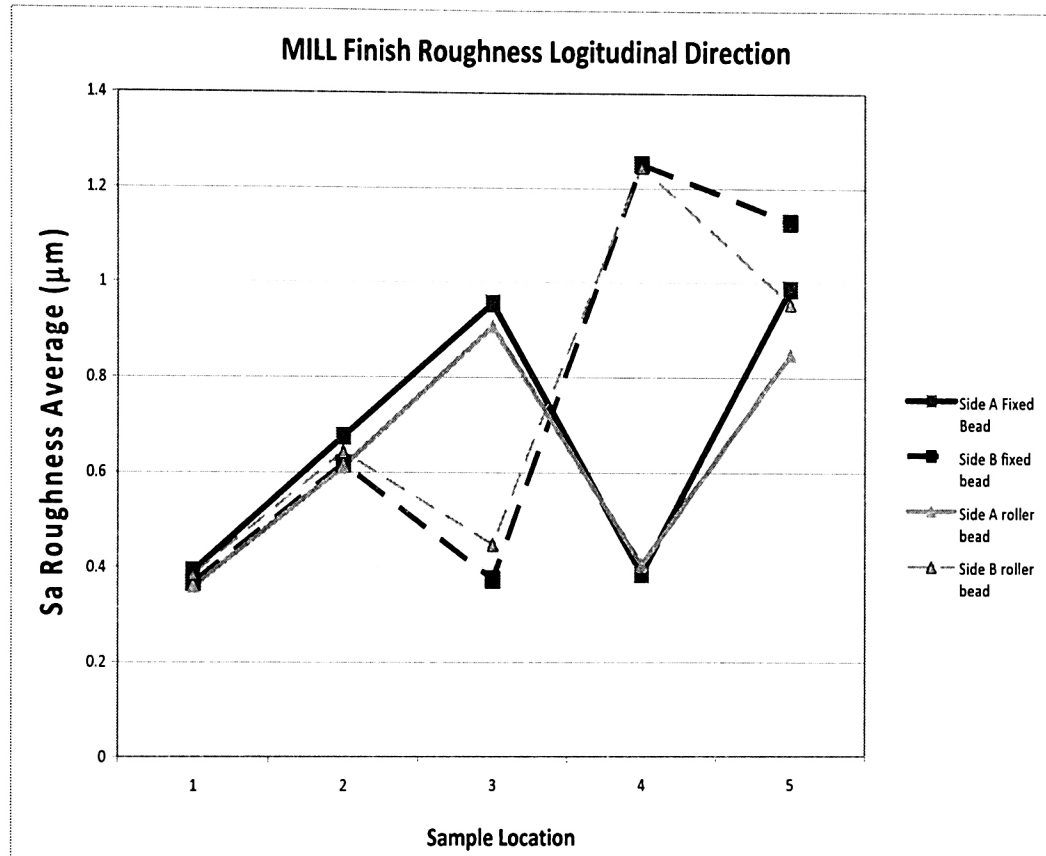


**Figure 20. MF Longitudinal Sa Roughness Evolution**

#### 4.2.3.3. EDT Transverse DBS Results

EDT textures are credited with improving paint and finishing quality, at a greater cost than MF textures. EDT textures have a Sa roughness amplitude over four times greater than MF. Sa data has been recorded at the five positions along the sample and presented in line graph form in Figure 21. The starting surface roughness values are slightly different for the four starting positions - sides A and B on both roller bead and fixed bead samples. For



comparison purposes, this was eliminated arithmetically, effectively translating each of the four curves up or down to a common starting position.

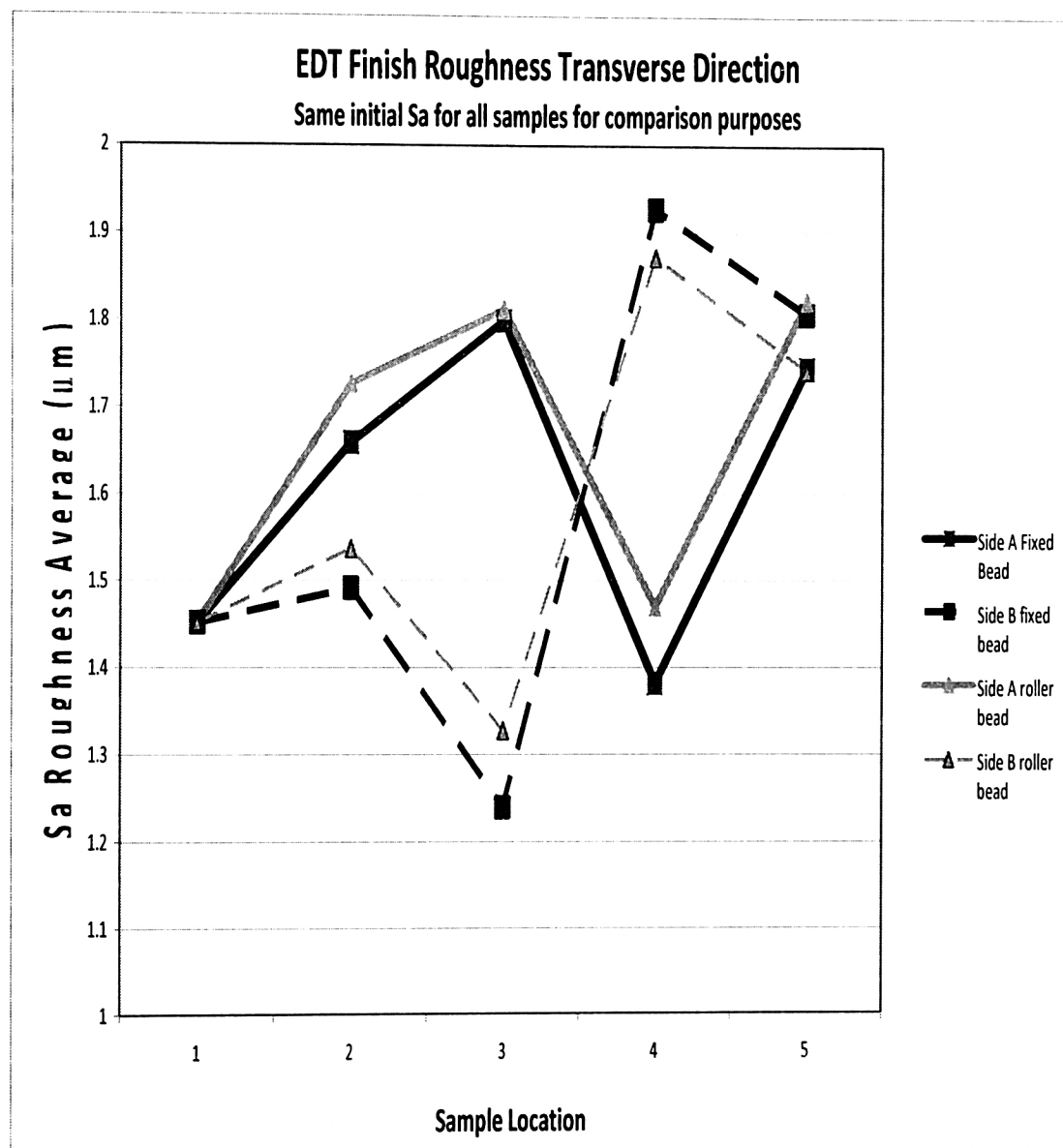


**Figure 21. EDT Transverse Sa Roughness Evolution**

During the passage of the sample over the first drawbead, both sides increase in roughness. It is interesting to note that the concave side A

increased in roughness by a much larger factor with its negative strain than the positively strained convex side B, even while under contact pressure from the first pin. As stated above for MF samples, the first pin correlated with Pure Bending results. This trend for EDT at the first bend is also shown to correlated with the corresponding Pure Bending result given in Figure 18.

As the sample contacts the second pin, the now convex side A is strained in the opposite direction, achieving a net positive strain, and reaching an even higher roughness value, while the now concave side B is strained negatively, and subjected to contact pressure. It falls far below its initial value. It is obvious that the effect of contact pressure is now a significant factor in affecting the surface roughness. As the material comes into contact with the third pin, the now convex side B strains in the positive direction and experiences a drastic increase in surface roughness. It should be noted that this location is subjected to the most extreme tensile stress and strain of any point during the entire operation. The now concave side A experiences a huge drop in surface roughness as it is strained negatively, returning to nearly starting roughness (slightly lower for fixed bead, slightly higher for roller bead). Contact forces are at their highest levels at this point, due to the occurrence of maximum net tensile force. At location 5, both sides are now free from contact with the third pin. Side B is strained negatively, although not enough

to give it a net negative strain. Side A is strained positively. Both sides are left with a net positive strain as the sample is now loaded with maximum total tensile stress. Side A experiences a huge increase in surface roughness, while side B falls slightly, which was at first unexpected in the absence of contact pressure.

#### **4.2.3.4. EDT Longitudinal DBS Results.**

The EDT Longitudinal results closely mirror the EDT Transverse result with a two noticeable exceptions (Figure 22). The drop in surface roughness for side B upon going from flat to convex in the transition from position 1 to 2 is unlike that of the EDT Transverse case. The drop in surface roughness for side A in going from convex to concave in the transition from 2 to three is also unlike that of the EDT transverse case. This observation may be explained by the bulk mechanical properties of the material and by variations on the EDT texture itself. The designation Longitudinal or Transverse is explained by the rolling direction at the steel mill. A longitudinal sample is DBS processed in the same direction as the direction of rolling. A transverse sample is processed at a 90 degree angle to that. This rolling process hardens the material anisotropically, making it more difficult to strain (stronger) in the

direction of rolling than in the transverse direction. This effect explains the increase in drawing load for longitudinal samples vs. transverse samples.

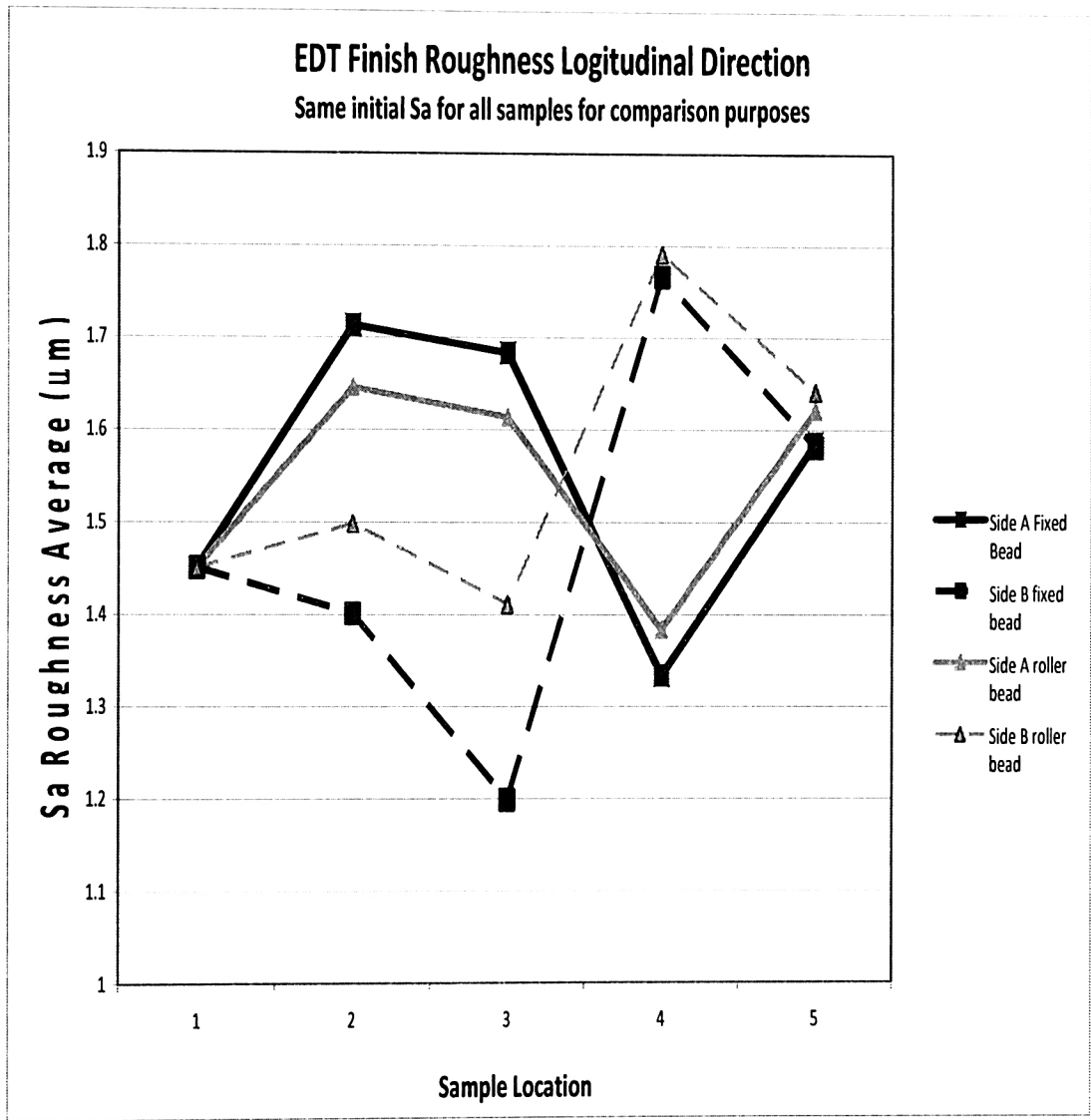


**Figure 22. EDT Longitudinal Sa Roughness Evolution**

The decrease in surface roughness for side B for the fixed bead case may also be influenced by the contact pressure exerted by the backup roller as it

reacts the moment created by bending the sample around the first pin. This contact pressure is larger than in the Transverse case because of the anisotropic hardening effect. There is an additional superimposed moment for the fixed case vs. the roller case created by the friction resisting the travel of the sample as it touches the first pin.

The second noticeable effect is the dropping of surface roughness as side A transitions from concave to convex as it moves from position 2 to position 3. The pure bending moment results suggest that the roughness will increase at this point. This may also be explained due to the increased contact force required to resolve the moment required to execute that bend. This contact force is more significant in flattening the surface features than the tensile straining is in promoting roughness.

#### **4.3. Plasticity Index Results**

A measure of the degree of plasticity inherent with the contact between two surfaces was developed by Bhushan [12]. It is expressed with equation 4.

$$\Psi = \left( \frac{E^*}{H} \right)^2 * \left( \frac{\sigma_p}{R_p} \right) \quad (4)$$

Where  $E^*$  is the effective modulus of the two surfaces in contact,  $H$  is the hardness of the material,  $\sigma_p$  is the standard deviation of peak heights, and  $R_p$  is the effective peak radius. Lower plasticity indices indicate that a surface is less likely to undergo plastic deformation. It can be observed that an increase in material hardness or effective peak radius will lower the plasticity index. The pure bending moment device gives us the opportunity to replicate the condition of the surface of the concave side 3B in the absence of contact pressure. The fourth datapoint in the pure bending data is the pure bending equivalent of concave side 3b having followed the same bending sequence. It was originally flat, then bent to convex, then bent to concave. We can evaluate the plasticity index of this region for the EDT and MF samples. This will allow us to gain insight into the potential for influence of roughness at these points due to contact pressure (Table III). The plasticity indices for the EDT textures are much higher than for the MF textures. This is reflected in

the reduction in surface roughness to levels below the starting roughness for DBS EDT samples.

Table IV. Plasticity index for uncontacted 3B

Condition	$\Psi$
EDT L	25.1432693
EDT T	29.0202701
MF L	16.4089938
MF T	14.9394187

## 5. Summary and Conclusions

This study investigated the evolution of surface roughness during DBS testing, pure bending moment testing, and uniaxial tensile testing. Friction results for DBS testing were also established.

The finding that friction for EDT textures was both larger, and more isotropic than EDT textures has been previously established by extensive testing. EDT drawing friction varied by only 6% from longitudinal to transverse directions. MF texture drawing friction varied by over 60% from longitudinal to transverse directions. The uniform directional friction characteristics make it a superior drawing material at a higher cost.

The primary mechanisms affecting surface roughness were proven to be tensile and compressive straining in addition to contact pressure. Friction effects were the least significant factor, with Sa differences between roller and fixed beads mostly unnoticeable.

The pure bending moment device offers capabilities that are especially unique in surface texture studies. Specific to the study of the DBS forming process, It is especially in useful in its ability to isolate certain strain conditions. The ability to subject materials to cyclic and compressive allows the investigation of new phenomena such as reversible roughening effects is also an important quality. Subjecting a MF longitudinal sample to a 10% compressive/tensile strain, the pure bending device causes an average increase in surface Sa value of 203%. Reversing the bend and returning the sample to a flat condition reduces the increase in Sa roughness to a mere 12%. This indicates a large degree of reversibility in the displacement field surface structure, which would otherwise be unrealized without using a device capable of such large reversing strains.

The behavior of EDT samples in pure bending was suprising in comparison to the behavior of MF textures. Subjecting a MF sample to pure bending causes both tensile and compressive sides to increase in surface roughness equally. Subjecting an EDT sample to pure bending causes an



average increase in roughness on the compressive side of 27%, but only a 13% increase on the tensile side. A through thickness orthotropy could be the source of this discrepancy. Further testing should be undertaken to study this effect.

The high flattening behavior of EDT textures in DBS contact areas in relation to MF involves both spatial and amplitude factors. The plasticity index evaluation indicates that the susceptibility of the EDT texture to contact flattening is a result asperity peak RMS and asperity peak radius. The plasticity index increases proportionately to the asperity peak RMS. The plasticity index is inversely proportional to the asperity peak radius. This suggests that the plasticity index could be reduced without decreasing the  $S_a$  roughness giving EDT textures their superior paintability. Increasing the asperity tip radius and more carefully controlling the asperity height distribution could reduce the plasticity index. This would allow EDT textures to retain more of their factory surface roughness while maintaining the friction and textural isotropy for which they are prized.

## Bibliography

- [1]C. Lahaye, et al., "Influence of Substrate Texture on Forming and Paint Appearance of Aluminum Sheet Material", *Proceedings of the International Body Engineering Conference IBEC' 97*, 1997.
- [2]J. Bottema, et al., "Recent Developments in AA6016 Aluminum Type Body Sheet Product", SAE Paper 981007, 1998.
- [3]M. Pfestorf, et al., "Three-dimensional characterization of surfaces for sheet metal forming", *Wear* 216 1998, 244-250
- [4]L.R. Sanchez et al., "An Analytical and Experimental Study of the Flow of Sheet Metal between Circular Drawbead", *ASME J. Engr. For Industry*, 1996, v118
- [5]Nine H., "Draw bead forces in sheet metal forming", Wang Koistinen, editor. *Mechanics of sheet metal forming*. New York, NY: Plenum Press; 1978. p. 179-211

- [6] Patir, N., and Cheng, H.S., 1979, "An Average Flow Model for Deterministic Effects of Three-dimensional Roughness on Partial Hydrodynamics Lubrication," ASME J. Lubr. Technol., 100(1), pp. 12-17
- [7] Per Carlsson, "Surface Engineering in Sheet Metal Forming", Acta Universitatis, Upsaliensis, Uppsala, 2005. ISBN 91-554-6136-0
- [8] D. Raabe, M. Sachtleber, H. Weiland, G. Scheele, Z. Zhao, Acta Mater. 51 (2003) 1539.
- [9] D. Raabe, M. Sachtleber, L.F. Vega, H. Weiland, Adv. Eng. Mater. 4(2002) 859.
- [10] R. Mahmudi, M. Mehdizadeh, J. Mater. Process. Technol. 80-81 (1998) 707.
- [11] D.V. Wilson, W.T. Roberts, P.M.B. Rodrigues, Metall. Trans. 12A (1981) 1603.

[12] Bhushan, B. (1998), "Contact Mechanics of Rough Surfaces in Tribology: Multiple Asperity Contact," Trib. Lett. 4, 1-35